

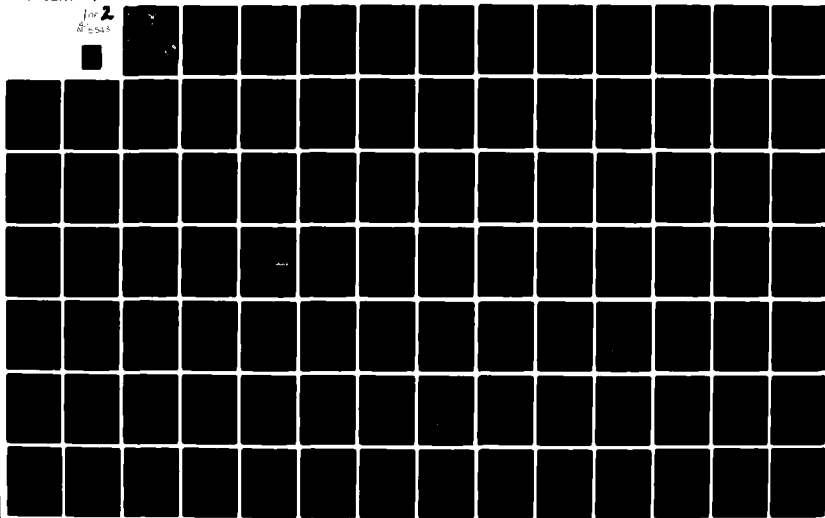
AD-A115 543

AIR FORCE INST OF TECH WRIGHT-PATTERSON AFB OH SCHOO--ETC F/8 17/8  
PREDICTION OF SHORT TERM TRACKING TASKS USING AN OPTIMAL PILOT --ETC(U)  
MAR 82 P A MULLEN  
AFIT/8AE/AA/81D-21

UNCLASSIFIED

NL

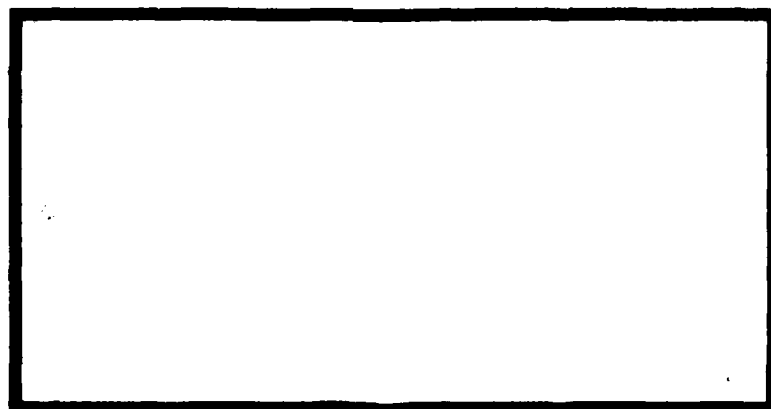
for 2  
Revised



①



AD A115543



DTIC  
ELECTE  
JUN 14 1982  
H

UNITED STATES AIR FORCE  
AIR UNIVERSITY  
**AIR FORCE INSTITUTE OF TECHNOLOGY**  
Wright-Patterson Air Force Base, Ohio

DTIC FILE COPY

DISTRIBUTION STATEMENT A  
Approved for public release;  
Distribution Unlimited

82 06 14 155

AFIT/GAE/AA/81D-21

①

PREDICTION OF SHORT TERM TRACKING TASKS  
USING AN OPTIMAL PILOT MODEL

THESIS

AFIT/GAE/AA/81D-21

Patrick A. Mullen  
Captain CAF

DTIC  
JUN 14 1982  
H

Approved for public release; distribution unlimited

AFIT/GAE/AA/81D-21

PREDICTION OF SHORT TERM TRACKING TASKS  
USING AN OPTIMAL PILOT MODEL

THESIS

Presented to the Faculty of the School of Engineering  
of the Air Force Institute of Technology  
Air University  
in Partial Fulfillment of the  
Requirements for the Degree of  
Master of Science

by

Patrick A. Mullen, B.Sc.

Captain

CAF

Graduate Aeronautical Engineering

March 1982

Approved for public release; distribution unlimited.

## Preface

I would like to take this opportunity to thank those who made it possible for me to complete this thesis.

My thanks first to the Canadian Armed Forces who gave me the opportunity to further my education. My sincere thanks also to my faculty advisor, Captain James T. Silverthorn who suggested the topic and guided my efforts throughout the project.

Special thanks to Mr. Ron Anderson from Air Force Wright Aeronautical Laboratory for sponsoring the thesis and to Mr. David Potts from the Air Force Systems Command Computing Services whose assistance with the hybrid simulation was outstanding. I would also like to thank my typist, Mrs. Cheryl Nicol, for the excellent work she performed.

Last, and for sure most, I wish to thank my wife for enduring the "seige" that was this thesis. Her support and understanding helped through it all.

Patrick A. Mullen



Accession For	
NTIS GRA&I	<input checked="checked" type="checkbox"/>
DTIC TAB	<input type="checkbox"/>
Unannounced	<input type="checkbox"/>
Justification	
By	
Distribution/	
Availability Codes	
Dist	Avail and/or Special
A	

## Contents

	Page
Preface . . . . .	ii
List of Figures . . . . .	v
List of Tables . . . . .	vii
List of Symbols . . . . .	viii
Abstract . . . . .	xii
I. Introduction . . . . .	1
Background . . . . .	1
Objective . . . . .	2
Analysis Procedure . . . . .	3
Limits and Assumptions . . . . .	4
Approach . . . . .	5
II. Lead Computing Optical Sight . . . . .	6
Fire Control Problem . . . . .	7
Related Kinematics . . . . .	13
Short Comings of the LCOS System . . . . .	14
III. Analog Simulation of the Air-to-Air Task . . . . .	16
Selection of System Variables . . . . .	16
Attacker Model . . . . .	16
Equations of Motion . . . . .	16
Elevator Actuation . . . . .	18
Target Modelling . . . . .	21
Generation of Target Motion . . . . .	21
Target Interface with System . . . . .	22
Target Kinematics . . . . .	24
Hybrid Computer . . . . .	25
Fixed Base Simulator . . . . .	26
Presentation of Task to Pilot . . . . .	27
Gathering of Data . . . . .	28
Data Reduction . . . . .	31
IV. Analytic Solution Using Optimal Model of the Human Controller . . . . .	33
Optimal Pilot Model . . . . .	33
An Overview . . . . .	33
Creating the Optimal Control . . . . .	36

## Contents

	Page
Optimal Estimator and Predictor . . . . .	40
System Statistics . . . . .	43
Application to the Air-to-Air Task . . . . .	43
The State Equations of Motion . . . . .	43
Determination of Noise Covariances . . . . .	46
Modelling Threshold Effects . . . . .	47
Target Motion Noise Covariance . . . . .	51
Cost Functional Weightings, $Q_x, r, q$ . . . . .	52
The Pilot Model in Action . . . . .	55
V. Analysis of Results . . . . .	57
VI. Conclusions and Recommendations . . . . .	66
Conclusions . . . . .	66
Recommendations . . . . .	68
Bibliography . . . . .	69
Appendix A: Determination of Projectile Time of Flight and Average Relative Velocity . . .	71
Appendix B: Algorithm Used to Generate White Noise Source . . . . .	76
Appendix C: Tabulation of Hybrid Simulation Results and of OPM Predicted versus Actual Hybrid Results . . . . .	77
Appendix D: Summary of Pilot Flying Experience . . . .	83

## List of Figures

<u>Figure</u>		<u>Page</u>
1	Air-to-Air Tracking as Seen by Attacker at Close Range . . . . .	7
2	Air-to-Air Tracking Geometry . . . . .	8
3	Functional Diagram of the Two Dimensional Air-to-Air Tracking Task . . . . .	17
4	Analog Schematic of the Attacker Aircraft Dynamics . . . . .	20
5	Filtered Input for Target Motion . . . . .	21
6	Analog Circuit for Target Flight Path Generation . . . . .	22
7	Analog Representation of Sight and Problem Kinematics . . . . .	23
8	Functional Diagram of Hybrid Computer . . . . .	24
9	Depiction of Simulator Cockpit Equipment . . . . .	25
10	Simulation Display . . . . .	26
11	Typical Tracking Performance of Input and Recorded Variables . . . . .	30
12	Functional Schematic of Optimal Pilot Model in the Control Loop . . . . .	34
13a	Equivalent First Order Lag Included to Model Neuromuscular Lag . . . . .	37
13b	Optimal Pilot Model (Closed Loop) with Equivalent Neuromuscular Lag Included . . . . .	38
13c	Optimal Pilot Model (Closed Loop) with First Order Lag and Correct Form of Optimal Input. . . . .	39
14	Computational Flow Diagram of the Optimal Pilot Model in the Control Loop (System Equations Augmented) . . . . .	42
15	Plot of Threshold Nonlinearity . . . . .	48



<u>Figure</u>		<u>Page</u>
16	Plot of Threshold Nonlinearity Equivalent Gain, $\hat{f}$ . . . . .	49
17	Visual Threshold Geometry . . . . .	50
18	Comparison of RMS Performance Results Between Reference and This Study . . . . .	58
19	RMS Performance Comparison Between OPM Predicted vs Actual Hybrid Using $Q_y$ Used for Long Term Tracking . . . . .	59
20	RMS Comparison of Performance Results Using $Q_y$ with Decreased Weighting on $\epsilon$ . . . . .	61
21	RMS Performance Comparison from OPM Modelled with Increased Observer and Motor Noise . . . . .	62
A-1	Projectile Trajectory Geometry . . . . .	72

## List of Tables

<u>Table</u>		<u>Page</u>
I	Dynamic Parameters and Stability Derivatives of Test Cases . . . . .	29
II	Tabulation of Hybrid Simulation Data- RMS Results from Three Test Pilots . . . . .	78
III	Tabulation of Predicted vs Actual Results-Original $Q_y$ Weighting Matrix . . . . .	79
IV	Tabulation of Predicted vs Actual Results- Decreased Weighting on $Q_{y\epsilon}$ Term . . . . .	80
V	Tabulation of Predicted vs Actual Results- Increased Observation and Motor Noise . . . . .	81
VI	Tabulation of Predicted vs Actual Results- INTEG vs MLINEQ . . . . .	82
VII	Summary of Pilot Experience . . . . .	83

### List of Symbols

Note: Underlined variables in this report indicate column vectors. Capital letters in vector equations are matrices.

$A$	System plant matrix
$\bar{A}_{z_T}$	Target acceleration normal to longitudinal axis
$\hat{a}_{x,z}$	Unit normal vectors in attacker body axes
$\underline{b}$	System control vector
$C$	Error Covariance matrix
$D$	Present range
$E\{\cdot\}$	Expected value operator
$F_s$	Force applied to control stick
$\hat{f}$	Visual threshold gain factor
$\underline{g}$	Gravity vector
$g$	Control rate weighting
$H$	System observation matrix
$J(\cdot)$	Cost functional
$K_B$	Ballistic parameter
$K_f$	Force stick sensitivity
$K_L$	Control linkage gain
$K_O$	Riccati gains
$k$	Viscous drag factor
$M_\alpha, M_\alpha^\bullet$	Aircraft stability derivatives relating pitching moment to angle of attack and angle of attack rate

$M_{\delta}$	Aircraft stability derivative relating pitching moment to elevator deflection
$M_q$	Aircraft stability derivatives relating pitching moment to pitch rate
0	Inertially fixed reference point
$Q_x$	State weighting matrix
$Q_y$	Weighting matrix for observed variables
$q$	Pitch rate of attacker
$r$	Control weighting
$\bar{r}_{B/0}$	Range of projectile from attacker firing position
$\bar{r}_{T/0}$	Range of target from attacker firing position
$s$	Laplace operator
$t$	Time
$T$	Tracking time in simulation
$T_f$	Projectile time of flight
$U_o$	Trim velocity
$u$	Pilot control input to system
$u_c$	Commanded control input
$\bar{v}_{A/0}$	Attacker velocity
$\bar{v}_f$	Mean relative velocity of the projectile over one time of flight
$\bar{v}_{B/A}$	Bullet muzzle velocity
$\bar{v}_{T/0}$	Target velocity
$v_u$	Covariance of motor noise

$V_y$	Covariance of observation noise
$\bar{V}_{avg}$	Average inertial bullet velocity
$v_u$	Motor Noise
$v_y$	Observation noise
$W$	Covariance of noise input to system dynamics
$w$	Noise input to system dynamics
$\underline{x}$	State vector
$\underline{y}$	Observation vector
$\underline{y}_p$	Noise-corrupted observation vector
$\underline{z}$	Augmented system state vector
$Z$	Covariance of $\underline{z}$
$Z_\alpha$	Aircraft dimensional stability derivative relating normal force to angle of attack
$Z_\delta$	Aircraft dimensional stability derivatives relating normal force to elevator deflection
$\alpha$	Angle of attack of attacker
$\gamma_A$	Flight path angle of attacker
$\gamma_T$	Flight path angle of target
$\delta$	Elevator deflection angle of attacker
$\delta(t-\sigma)$	Kronecker delta function
$\delta_c$	Commanded elevator deflection angle
$\epsilon$	Tracking error angle
$\underline{\zeta}$	Dummy state vector used in predictor
$\underline{n}$	Vector of dummy variables, $= CH_1^T V_y^{-1} \underline{y}_p + \underline{b}_1 e^{-s\tau} u_c$

$\theta$	Pitch angle of attacker
$\underline{l}$	Optimal feedback gains
$\lambda$	Lead angle
$\mu$	Noise-corrupted commanded control input
$\rho$	Atmospheric density
$\rho_0$	Sea level atmospheric density
$\rho_i, \rho_u$	Constants for computation of noise covariance
$\Sigma_p$	Inertial angular position of sight reticle
$\Sigma_T$	Inertial line of sight (LOS) angle from attacker to target
$\Sigma_{TA}$	Relative line of sight angle from attacker to target
$\sigma$	Dummy variable of integration
$\sigma_x$	RMS value of $x$
$\tau$	Pilot time lag
$\tau_a$	Time constant of actuator
$\tau_N$	Pilot neuro-muscular time constant
$\tau_T$	Target time constant
$\bar{\omega}_{LOS}$	Inertial angular velocity vector of line of sight

## Abstract

An optimal pilot model has previously been successful in predicting the long term tracking performance of a longitudinal air-to-air gunnery task. This study investigated modifications to the same pilot model to determine whether it could be used to successfully predict performance for a short term task.

The same task, including a lead computing optical sight, was simulated on a hybrid computer. Three pilots flew three different aircraft configurations on the fixed-base simulator against a target driven to RMS accelerations of 3.5G and 5.0G by filtered, Gaussian noise. The target was at either 1000' or 3000' range. Averaged RMS data were recorded on the attacker's elevator deflection, pitch rate, lead angle, line of sight angle, and tracking error for each case.

The identical task was modelled and analyzed using a digital pilot model formulated from optimal control theory. Modifications to this pilot model were made to reflect the short term tracking assignment. A comparison of the data generated by the human pilots versus that of the optimal pilot model showed moderate correlation for elevator deflection, lead angle and pitch rate. There was less correlation for line of sight and tracking error although the pilot model usually predicted the correct ranking of performance.

cont

Overall, the optimal pilot model was less successful in predicting short term tracking performance than it was in predicting long term performance.



# PREDICTION OF SHORT TERM TRACKING TASKS USING AN OPTIMAL PILOT MODEL

## I. Introduction

### Background

Many systems designed today require human operator activity to maintain system control. In some instances marginally stable systems may become unstable due to inherent complexities and imperfections introduced by the human operator. To avoid costly redesign problems in the final stages of implementation, effort is made to simulate the complete system, including the control function performed by the human operator.

These simulations take one of two forms. The first is direct simulation on analog or hybrid computers. This demands human input to close the control loop as in the real system. The second method involves mathematical simulation of the operator as well as the controlled system so as to allow prediction of human operator reaction to system design and evaluation of the performance of the closed loop system. The latter method, if successful, alleviates the need for repetitive data collection required when the human operator is used in the simulation; to be successful the model must accurately duplicate the performance of the human operator.

Various models have been developed for this purpose.

To accommodate the human controller task to be examined in this study, the optimal pilot model, initially developed by Kleinman, Baron, Miller, Elkind, and Levison (Ref 2) will be used. It shall hereafter be referred to as the Optimal Pilot Model (OPM). It consists of a Kalman filter, state predictor and optimal feedback gains to simulate the analytical and anticipatory tasks which must be performed by a pilot to control his aircraft.

Harvey (Ref 1) showed that for a long-term tracking task (100 seconds) accurate prediction could be achieved for the performance of integrated aircraft flight control and lead computing optical sight (LCOS) systems. Schmidt (Ref 13) replicated the above results and extended the approach to this optimal design of control augmentation for long term tracking tasks. Unfortunately, not many human operator tasks are long-term tasks and this is especially so in fighter-on-fighter tracking assignments that occur in aerial gunnery where the attacker has relatively little time (5-10 seconds) to line up the target and accomplish his mission.

The question to be addressed in this thesis is whether the OPM developed for long-term tracking can be used to predict system performance for a short-term task (5-10 seconds).

### Objective

The objective of this study is to determine the correlation in performance for short-term tracking assignments

between that predicted by the OPM developed for a long-term tracking and that obtained using fixed base pilot-in-the-loop analog simulation.

#### The Analysis Procedure

The same basic procedure used by Harvey in Ref 1 to match OPM performance predictions with pilot-in-the-loop analog results of the air-to-air combat tracking task was used in this study. First data was gathered on actual pilot performance in this task via system simulation on the EAI 2000 Hybrid/MODCOMP Classic IV computer facility. Three pilots with previous fighter experience were presented a short-term tracking task as detailed in the simulation description in Section III and statistical data was recorded to reflect pilot performance of the task confronted in each experimental case.

The second simulation used the computer code constructed by Enright (Ref 5) based on the Kleinman subroutines (Ref 4) developed for OPM simulation and was run on the CDC CYBER 750 digital computer. The same statistical data on performance was collected and compared with that obtained from the hybrid simulation. The results of the comparison are listed in Section V of this report.

To obtain a large enough spread in the data to accentuate the correlation between analog and digital results, several different aircraft, ranging from good to bad handling qualities

for this task, were used. For each aircraft two different tracking ranges and target "G" loadings were simulated. The cases were the same as in Ref 1.

#### Limits and Assumptions

In keeping with Harvey's efforts the following limits and assumptions were applied:

a) only longitudinal tracking was modelled. This simplified model neglects the inertial cross coupling of the aircraft longitudinal, lateral, and yaw axes but yet supplies a model that will afford realistic results and still be easily simulated;

b) the problem was initiated with the attacker already in the tracking position relative to the target. The task is thus to continue tracking the target as closely as possible;

c) the attacking aircraft was considered rigid and unaffected by excessive normal "G" loadings in the interest of tracking the target with minimum error;

d) the attacker aircraft was assumed to maintain constant speed under any conditions of "G" loading, angle of attack or attitude;

e) the attacker and target were assumed to be flying at the same speed which, coupled with the geometry of the engagement, produced zero closing rate. Furthermore, the only evasive maneuver available to the target was to generate normal acceleration;

f) all dynamic equations used were linearized about the aircraft stability axes consistent with the linear nature of the OPM. Any perturbations were assumed sufficiently small to justify use of this linear approach in a nonlinear environment; and

g) the aircraft stability derivatives were assumed constant throughout the tracking task which is valid given the constant Mach number.

### Approach

This thesis is presented in seven parts. Chapter I provides a background to the pilot model and introduces its application to the air-to-air target tracking task. Chapter II provides a development of the Lead Computing Optical Sight and its related kinematics. In Chapter III the analog simulation of the task is explained followed by a development of the actual Optimal Pilot Model in Chapter IV. Chapter V presents the results and Chapter VI lists the conclusions and recommendations resulting from this study. The appendices contain pertinent derivations, a listing of the random number source used and the tabulated results.

## II. The Lead Computing Optical Sight

The task of accurately tracking a maneuvering target for the purpose of obtaining a "kill" with an airborne cannon is one of the most difficult required of a fighter pilot. As is the case when firing any projectile at a moving target, lead for target motion must be computed and the aiming direction adjusted to compensate for the target's motion during the projectile's time of flight. Further complicating the air-to-air tracking task are attitude adjustments that must be made to account for projectile drag, velocity jump, and gravity drop along the projectile's flight trajectory. It is the Lead Computing Optical Sight (LCOS) on board the aircraft that performs this task of computing the necessary lead.

Lead angle is normally presented to the pilot of the attacking aircraft via pipper position on a Head-Up-Display. The pipper position is best thought of as a pseudo target for which the gun is correctly aimed. That is, if the pipper and target remain superimposed, the projectile will intercept the target's flight path. If the attacker aircraft is maneuvered so as to keep the pipper on the target then he has achieved the proper aiming direction, or lead angle to ensure a kill given that the target maneuver remains constant. The pipper position is displayed on the HUD as a dot within a small circle depressed from the attacker weapon line by the lead angle,  $\lambda$ . Figure 1 shows a typical view as would be seen by the attacker in an actual fighter-on-fighter tracking situation.

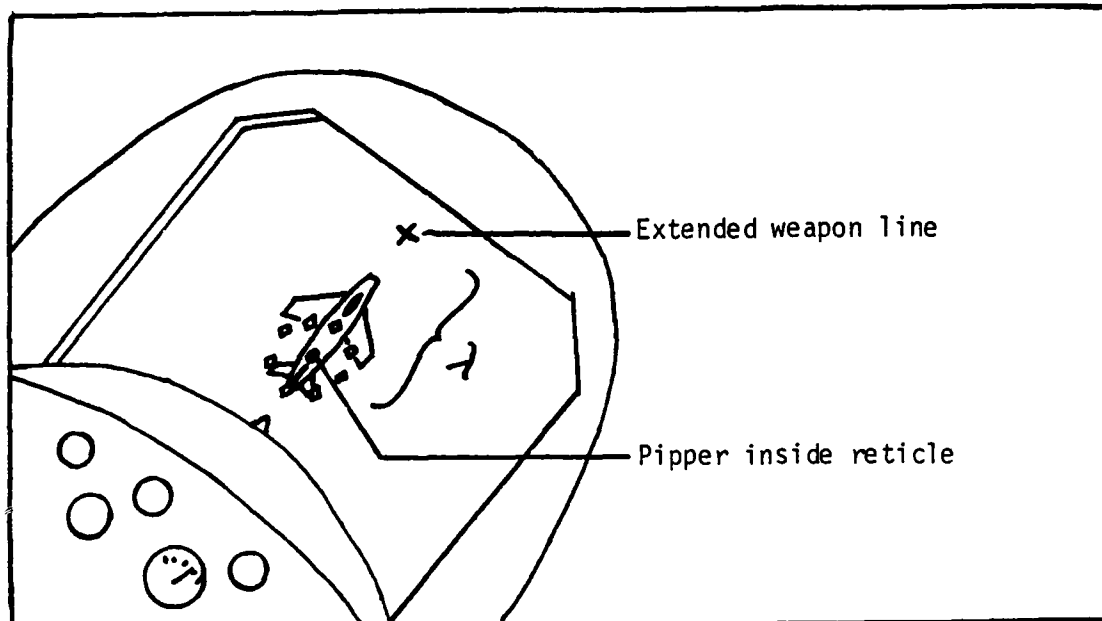


Figure 1. Air-to-Air Tracking as Seen by Attacker at Close Range

#### Fire Control Problem

Calculation of the lead angle consists of solving the basic fire control problem. This requires that the projectile intercept the target at some future point in the target's flight trajectory so that at  $t = t_0 + T_f$

$$\bar{r}_{B/O}(t_0 + T_f) = \bar{r}_{T/O}(t_0 + T_f) \quad (1)$$

where  $t_0$  is the present time,  $T_f$  is the time of flight to intercept and  $\bar{r}_{B/O}(t_0 + T_f)$  and  $\bar{r}_{T/O}(t_0 + T_f)$  are the future positions of the bullet and target respectively at intercept. Expressions for these quantities may be obtained by referring to the air-to-air, in plane tracking geometry depicted in Fig 2. The variables are defined as

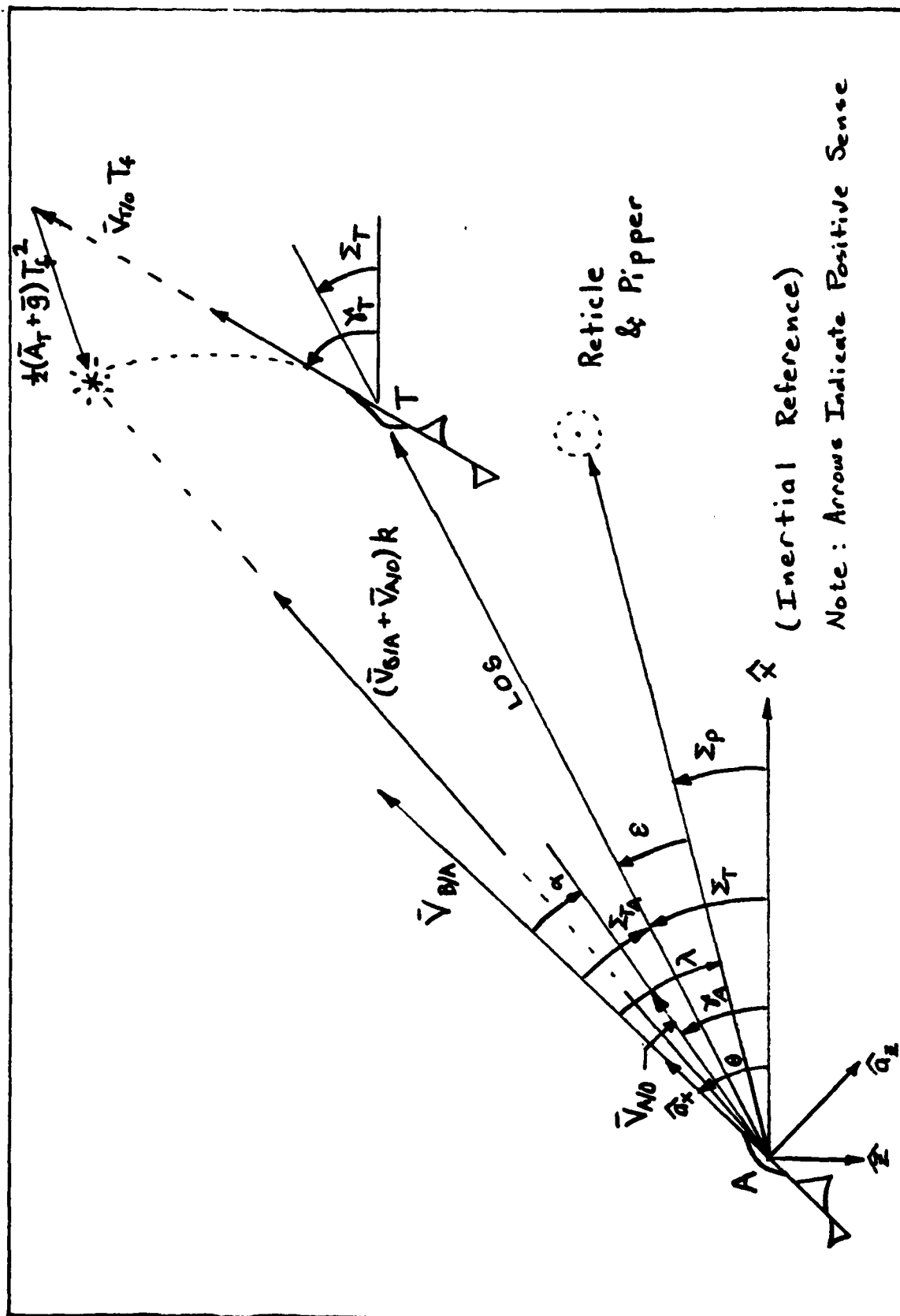


Figure 2. Air-to-Air Tracking Geometry



- $\lambda$  = lead angle  
 $\alpha$  = angle of attack of attacker  
 $\dot{\Sigma}_T$  = inertial angular rate of Line of Sight (LOS) from attacker to target  
 $\dot{\Sigma}_P$  = inertial angular rate of pipper  
 $\hat{a}_{x,z}$  = unit normal vectors in attacker body axes  
 $\bar{A}_T$  = target specific acceleration (i.e. not including gravity)  
 $\bar{V}_{A/0}$  = attacker velocity relative to inertially fixed reference point 0  
 $\bar{V}_{T/0}$  = target velocity  
 $\bar{V}_{B/A}$  = bullet muzzle velocity  
 $k$  = drag scaling factor used in calculation of average relative bullet velocity,  $V_f$   
 $\epsilon$  = tracking error

By assuming constant target acceleration, the intercept positions of the target and bullet at  $T_f$  in the future may be written as

$$\bar{r}_{T/0}(t_o + T_f) = \bar{r}_{T/0}(t_o) + \bar{V}_{T/0}(t_o)T_f + \frac{1}{2}(\bar{A}_T + \bar{g})T_f^2 \quad (2)$$

$$\bar{r}_{B/0}(t_o + T_f) = \bar{r}_{B/0}(t_o) + (\bar{V}_{B/A} + \bar{V}_{A/0})kT_f + \frac{1}{2}\bar{g}T_f^2 \quad (3)$$

Since all these variables are calculated at the present time  $t_o$ , the argument  $t_o$ , will not be used hereafter.

Substituting (2) and (3) into equation (1) and dropping the common gravity terms, the intercept position becomes

$$\bar{r}_{B/0} + (\bar{V}_{B/A} + \bar{V}_{A/0})kT_f = \bar{r}_{T/0} + \bar{V}_{T/0}T_f + \frac{1}{2}\bar{A}_T T_f^2 \quad (4)$$

In general equation (4) is not satisfied since it assumes that the aircraft is aimed with correct lead angle  $\lambda$ , to bring about an intercept. At this point, however,  $\lambda$  is unknown to the aircraft or pilot. What is known is that the pipper position, to be displayed on the HUD via calculations made by the LCOS, represents a pseudo target for which the aircraft is correctly aimed. Thus by keeping the pipper on the target, the pilot is able to correctly aim his aircraft to cause an intercept.

Mathematically, this amounts to replacing the subscript "T" for target in the position term of equation (4) with a "P" for pipper so that

$$\begin{aligned}\bar{r}_{P/B} &= \bar{r}_{P/O} - \bar{r}_{B/O} \\ &= (\bar{v}_{B/A} + \bar{v}_{A/O})kT_f - (\bar{v}_{T/O}T_f + \frac{1}{2}\bar{a}_T T_f^2)\end{aligned}\quad (5)$$

In terms of the lead angle,  $\lambda$ , and the present range,  $D$ , the vector  $\bar{r}_{P/B}$  can be expressed as

$$\begin{aligned}r_{P/B}(t_o) &= D \cos\lambda \hat{a}_x + D \sin\lambda \hat{a}_z \\ &\approx D \hat{a}_x + D\lambda \hat{a}_z\end{aligned}\quad (6)$$

Equating the  $\hat{a}_z$  components of (5) and (6) gives

$$D\lambda = \{(\bar{v}_{B/A} + \bar{v}_{A/O})kT_f - (\bar{v}_{T/O}T_f + \frac{1}{2}\bar{a}_T T_f^2)\} \cdot \hat{a}_z \quad (7)$$

$\bar{v}_{B/A}$  and  $\bar{v}_{A/O}$  are known by the attackers LCOS and from Fig 2

are given by

$$\begin{aligned}\bar{V}_{B/A} + \bar{V}_{A/0} &= V_{B/A} \hat{a}_x + V_{A/0} (\cos \alpha \hat{a}_x + \sin \alpha \hat{a}_z) \\ &\approx (V_{B/A} + V_{A/0}) \hat{a}_x + \alpha V_{A/0} \hat{a}_z\end{aligned}\quad (8)$$

$\bar{V}_{T/0}$  and  $\bar{A}_T$ , however, are unknown. The velocity  $\bar{V}_{T/0}$  is written as

$$\begin{aligned}\bar{V}_{T/0} &= \frac{d}{dt}(\bar{r}_{T/0}) = \frac{d}{dt}(\bar{r}_{T/A} + \bar{r}_{A/0}) \\ &= (\dot{\bar{r}} + \bar{\omega}_{LOS} \times \bar{r}_{T/A}) + (\bar{V}_{A/0})\end{aligned}\quad (9)$$

where  $\dot{\bar{r}}_{T/A}$  is the rate of change of the relative position vector,  $\bar{r}_{T/A}$ , as observed in a rotating LOS frame and  $\bar{\omega}_{LOS}$  is the angular velocity vector of this frame. It is obvious from Fig 2 that  $\dot{\bar{r}}_{T/A}$  is simply the range rate vector, assumed zero in this study. With  $\bar{\omega}_{LOS}$  equal to  $\dot{\hat{\Sigma}}_T \hat{a}_y$ ,  $\bar{V}_{T/0}$  becomes

$$\begin{aligned}\bar{V}_{T/0} &= \bar{V}_{A/0} + [0 + \dot{\hat{\Sigma}}_T \hat{a}_y \times (\cos \lambda \hat{a}_x + \sin \lambda \hat{a}_z) D] \\ &= V_{A/0} (\cos \alpha \hat{a}_x + \sin \alpha \hat{a}_z) + \dot{\hat{\Sigma}}_T D (-\cos \lambda \hat{a}_z + \sin \lambda \hat{a}_x) \\ &\approx (V_{A/0} + \dot{\hat{\Sigma}}_T D \lambda) \hat{a}_x + (V_{A/0} \alpha - \dot{\hat{\Sigma}}_T D) \hat{a}_z\end{aligned}\quad (10)$$

The target's inertial LOS rate,  $\dot{\hat{\Sigma}}_T$  cannot be directly measured by the attacker LCOS but by assuming that the pipper closely tracks the target, one can approximate that

$$\dot{\hat{\Sigma}}_P \approx \dot{\hat{\Sigma}}_T \quad (11)$$

Thus  $\bar{V}_{T/0}$  becomes

$$\bar{V}_{T/0} = (V_{A/0} + \dot{\hat{\Sigma}}_P D \lambda) \hat{a}_x + (\bar{V}_{A/0} \alpha - \dot{\hat{\Sigma}}_P D) \hat{a}_z \quad (12)$$

To express  $\dot{\hat{\Sigma}}_P$  in terms of system variables, one sees from Fig 2 that

$$\dot{\hat{\Sigma}}_P = \dot{\hat{\theta}} - \dot{\lambda} = q - \dot{\lambda} \quad (13)$$

To obtain  $\bar{A}_T$  it is usually assumed that to track the target the attacker must generate the same normal acceleration as the target, so

$$\bar{A}_T \cdot \hat{a}_z \approx \bar{A}_A \cdot \hat{a}_z = A_z \quad (14)$$

where  $A_z$  represents the output of a center of gravity positioned normal accelerometer on board the attacker aircraft. The output of this accelerometer can be expressed in terms of the aircraft angle of attack,  $\alpha$ , by noting that

$$A_z = Z_\alpha \alpha + Z_\delta \delta$$

where  $Z_\alpha$  and  $Z_\delta$  are the dimensional stability derivatives (Ref 3:413).

In the high "G", high angle of attack environment that exists in aerial dogfight conditions

$$Z_\alpha \alpha \gg Z_\delta \delta$$

so that

$$A_z \approx Z_\alpha \alpha \quad (15)$$

Substituting (8), (12), (13), (14), and (15) into (7) gives

$$D\dot{\lambda} = \alpha V_{A/0} T_f (k-1) + (q - \dot{\lambda}) D T_f - \frac{Z_{\alpha} T_f^2}{2} \alpha$$

Dividing through by  $T_f D$  and noting from Appendix A that the average relative velocity of the bullet,  $V_f$ , is given by  $D/T_f$ , the equation governing the lead angle  $\lambda$  becomes finally

$$\dot{\lambda} = -\frac{1}{T_f} \lambda + q - \frac{1}{V_f} \left[ \frac{Z_{\alpha}}{2} - \frac{V_{A/0} (k-1)}{T_f} \right] \alpha \quad (16)$$

#### Related Kinematics

The inertial LOS rate of the target with respect to the attacker,  $\dot{\Sigma}_T$ , is computed from equation (9) by noting that

$$\dot{\bar{r}}_{T/A} + \bar{\omega}_{LOS} \times \bar{r}_{T/A} = \bar{V}_{T/0} - \bar{V}_{A/0} \quad (17)$$

The RHS of (17) is the target relative velocity while the LHS shows that this vector consists of two parts:  $\dot{\bar{r}}_{T/A}$  represents the component of the relative velocity along the LOS while  $\bar{\omega}_{LOS} \times \bar{r}_{T/A}$  is the component perpendicular to the LOS. Therefore in the planar case of this study  $\dot{\Sigma}_T$  can be written as the relative velocity perpendicular to LOS divided by the range, D. From Fig 2 it follows that

$$\dot{\Sigma}_T = \frac{V_{T/0}}{D} \sin(\gamma_T - \Sigma_T) - \frac{V_{A/0}}{D} \sin(\lambda - \alpha - \epsilon) \quad (18)$$

Using small angle assumptions and noting from Fig 2 that

$$\epsilon = \Sigma_T - \Sigma_P = \Sigma_T - \theta + \lambda$$

Thus

$$\dot{\Sigma}_T = \left(\frac{V_{A/O}}{D}\right)\alpha + \left(\frac{V_{A/O} - V_{T/O}}{D}\right)\Sigma_T + \left(\frac{V_{T/O}}{D}\right)\gamma_T - \left(\frac{V_{A/O}}{D}\right)\theta \quad (19)$$

Since allowing a rate of change of range,  $D$ , would result in time varying coefficients, the cases considered in this study were limited to zero closure rate with velocities of the attacker and target assumed constant and equal. Consequently, the second term in (19) was assumed zero in this study.

It was later necessary to modify this zero closure rate assumption slightly. A minimal amount of negative feedback was added to the  $\Sigma_T$  term of (19) in order to obtain a convergent solution to the Ricatti equation used; Section IV further explains this.

#### Short-comings of the LCOS System

Once the attacker is in a tracking position on the target (normally behind and slightly elevated in the target's plane of motion), he must then generate an angular rate of turn in that plane approximately equal to that of the target. The major tracking problem with the LCOS system arises when the attacker does not have the sight on the target. For instance, if the sight is behind the target the pilot must increase his turn rate to catch up. This results in an

erroneous increase in the displayed lead angle, leaving the pilot with no valid information as to exactly where to position his aircraft until his rate of turn is once again constant and equal to that of the target. A process of "hunting" then ensues until the pilot has either found the exact solution or decides to hold one solution steady and fire continuously while allowing the sight to "slide through" the target. In practice, the latter procedure usually leads to the best results. As is evident from equation (16), increasing the range causes the sight time constant,  $T_f$ , to become larger which in turn causes these unwanted dynamics to become even worse. Normally, the sight is designed with a nominal time constant based upon a nominal firing range of around 1500 feet (Ref 1:13) because for ranges much greater than this, sight performance becomes marginal.

The sight time constant for each case in this study was computed based upon the given tracking conditions.

### III. Analog Simulation of the Air-to-Air Task

The purpose of the analog computer simulation was to gather actual "pilot-in-the-loop" data on specific performance parameters for the air-to-air fighter tracking task. This data would then be compared with similar data generated from digital computer runs of the identical task flown by the analytical pilot model.

A system model of this task can be divided into five functional areas, as shown in Fig 3: the pilot (or pilot model), the flight control response, the aircraft equations of motion, the sight computer and its related kinematics. The remaining areas of this model and their implementation on the hybrid computer are discussed in this chapter.

#### Selection of System Variables

The same variables chosen by Harvey to describe the tracking task were used in this study, namely

$\delta$ = elevator deflection	$\lambda$ = lead angle
$\theta$ = pitch angle	$\Sigma_T$ = inertial line of sight angle
$q$ = pitch rate	$\bar{A}_{zT}$ = normal target acceleration
$\alpha$ = angle of attack	$\gamma_T$ = target flight path angle

#### The Attacker Model

Equations of Motion. As mentioned previously in the introduction, the equations of motion of the attacking



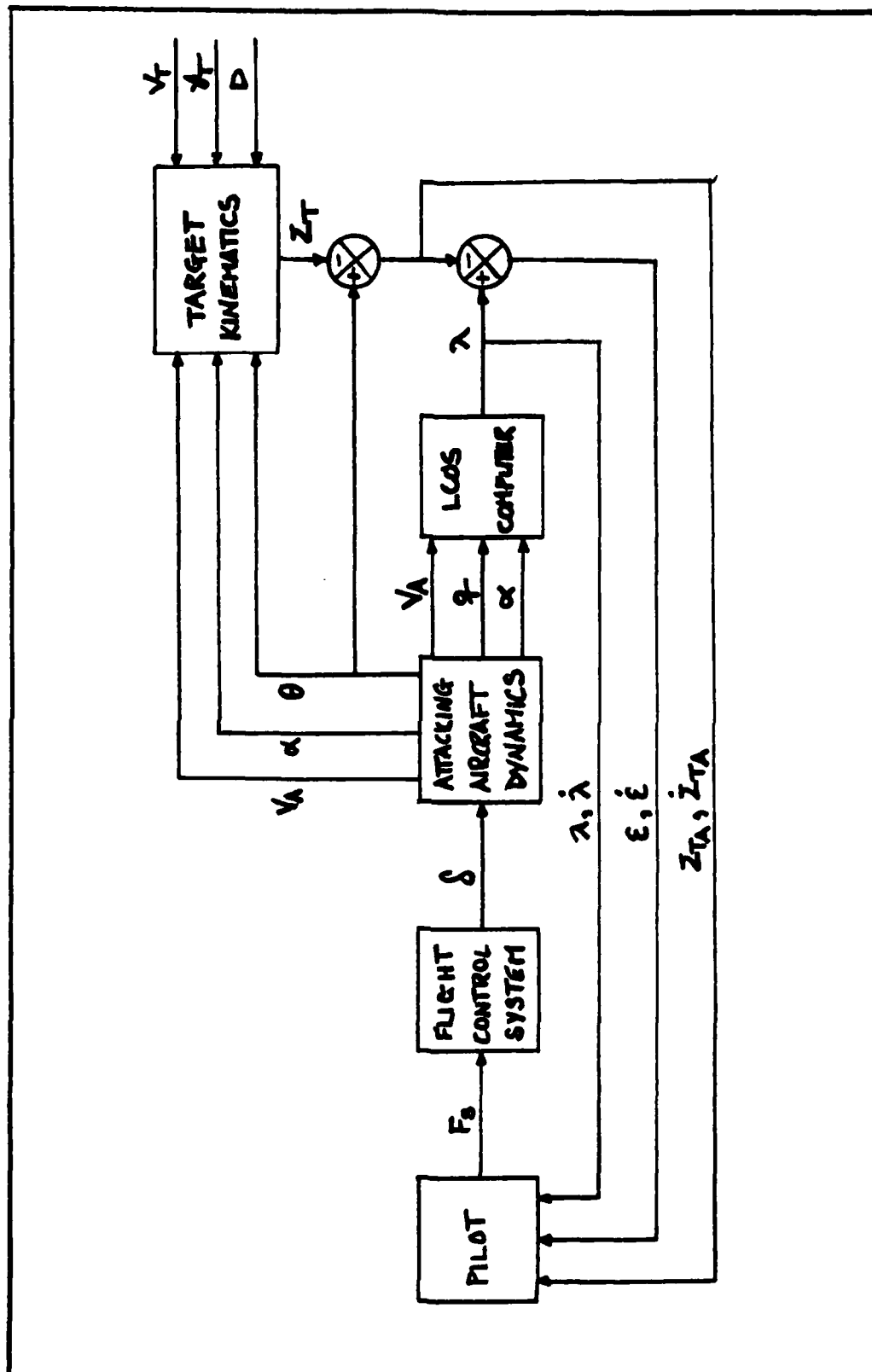


Figure 3. Functional Diagram of the Two Dimensional Air-to-Air Tracking Task.

aircraft were approximated by the standard "short period" stability axes equations. These equations are first-order, linear, and, in view of the assumption of constant stability derivatives, time-invariant differential equations which approximate aircraft response to control inputs. Since this analysis is concerned only with the longitudinal axis dynamics, only three equations are necessary. Those describing pitch angle, angle of attack, and pitch rate are respectively (Ref 3:414)

$$\dot{\theta} = q \quad (20)$$

$$\dot{\alpha} = q + \frac{Z_{\alpha}}{U_0} \alpha + \frac{Z_{\delta}}{U_0} \delta \quad (21)$$

and

$$\dot{q} = M_q q + M_{\alpha} \alpha + M_{\dot{\alpha}} \dot{\alpha} + M_{\delta} \delta \quad (22)$$

Substituting (21) into (22) and rearranging gives

$$\dot{q} = (M_{\delta} + M_{\dot{\alpha}} Z_{\delta} / U_0) \delta + (M_q + M_{\dot{\alpha}}) q + (M_{\alpha} + M_{\dot{\alpha}} Z_{\alpha} / U_0) \alpha \quad (23)$$

### Elevator Actuation

The transfer function relating elevator deflection,  $\delta$ , to commanded elevator input,  $\delta_c$ , for a typical tactical fighter aircraft is given by

$$\frac{\delta}{\delta_c} = \frac{k_L}{\tau_a s + 1} \quad (24)$$

where  $K_L$  is the control linkage gain and  $\tau_a$  is the time constant of the power cylinder actuator. Typical values for these two parameters are 0.8 (dimensionless) and 0.05 seconds, respectively. The differential equation for elevator deflection is then

$$\dot{\delta} = -\frac{1}{\tau_a} \delta + \frac{K_L}{\tau_a} \delta_c \quad (25)$$

The analog simulation utilized a force stick obtained from the Air Force Flight Dynamics Laboratory, Wright-Patterson Air Force Base. It provided the elevator control input to the simulation by converting pilot force in pounds to volts. The analog computer then converted this to the commanded elevator input  $\delta_c$ , using appropriate scaling factors where

$$-\delta_c = K_f F_s \quad (26)$$

The stick force sensitivity,  $K_f$  is in units of radians per pound force. Its value was determined after calibration of the force stick and after repeated trial tracking runs to find a value of  $K_f$  that provided the pilot with realistic tracking capability. The value chosen was 0.005 rad/lb. The negative sign in (26) results from the standard convention of assigning positive elevator deflection to that movement which results in negative pitch rate, i.e. "down" elevator. Substituting (26) into (25) gives

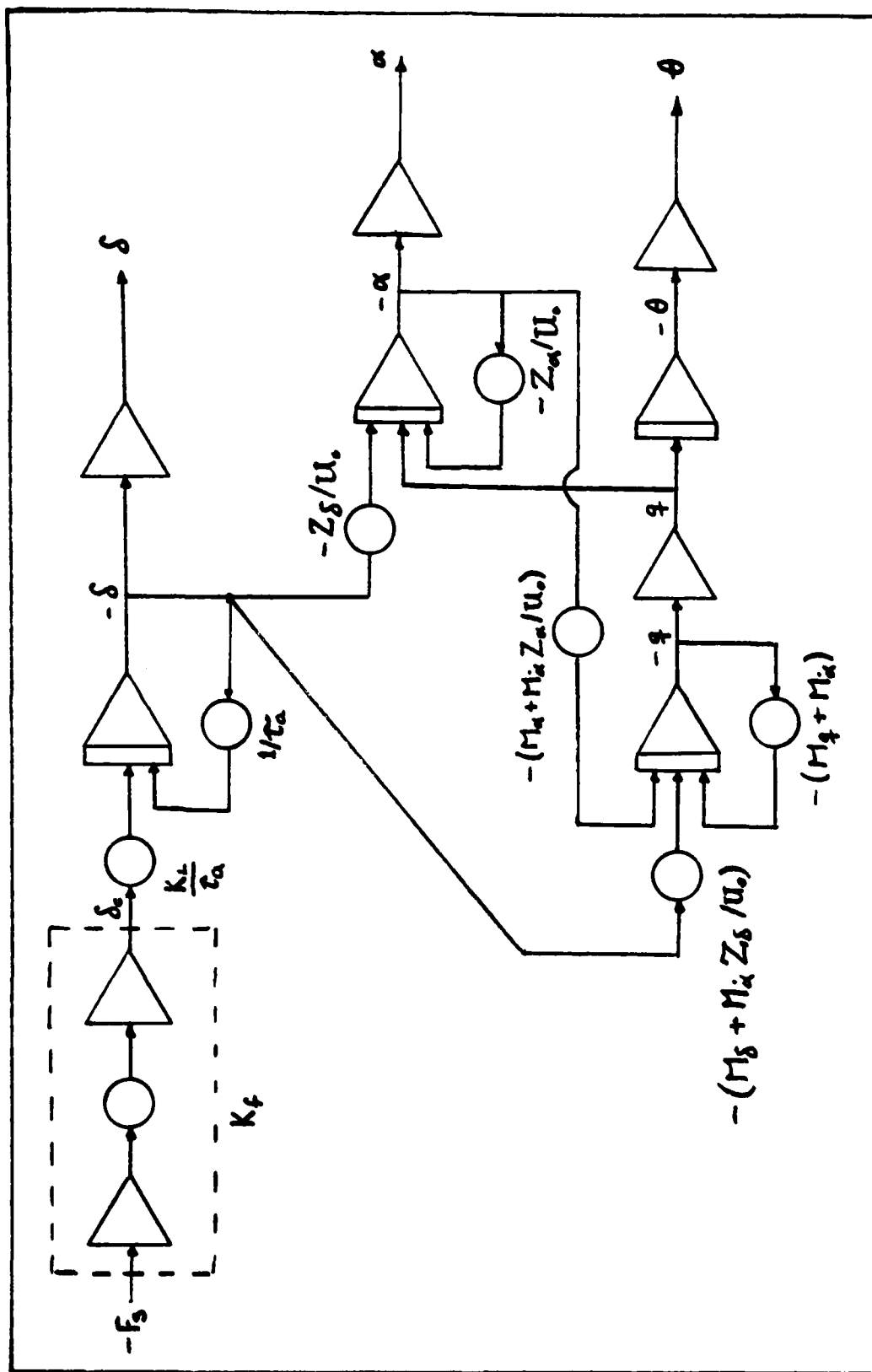


Figure 4. Analog Schematic of the Attacker Aircraft Dynamics.

$$\dot{\delta} = -\frac{1}{\tau_a} \delta - \frac{K_L K_f}{\tau_a} F_s \quad (27)$$

Figure 4 is the analog schematic of the attacking aircraft dynamics.

### Target Modelling

Generation of Target Motion. The target aircraft was modelled as a fighter possessing performance capabilities at least as strong as those of the attacker. Target normal acceleration,  $A_{z_T}$ , was derived from frequency-shaped Gaussian noise with statistics of zero mean and standard deviations of 3.5G or 5.0G for each case. The noise was obtained digitally on the hybrid computer using a random number generator function as an input to an algebraic algorithm (Ref 8:933)

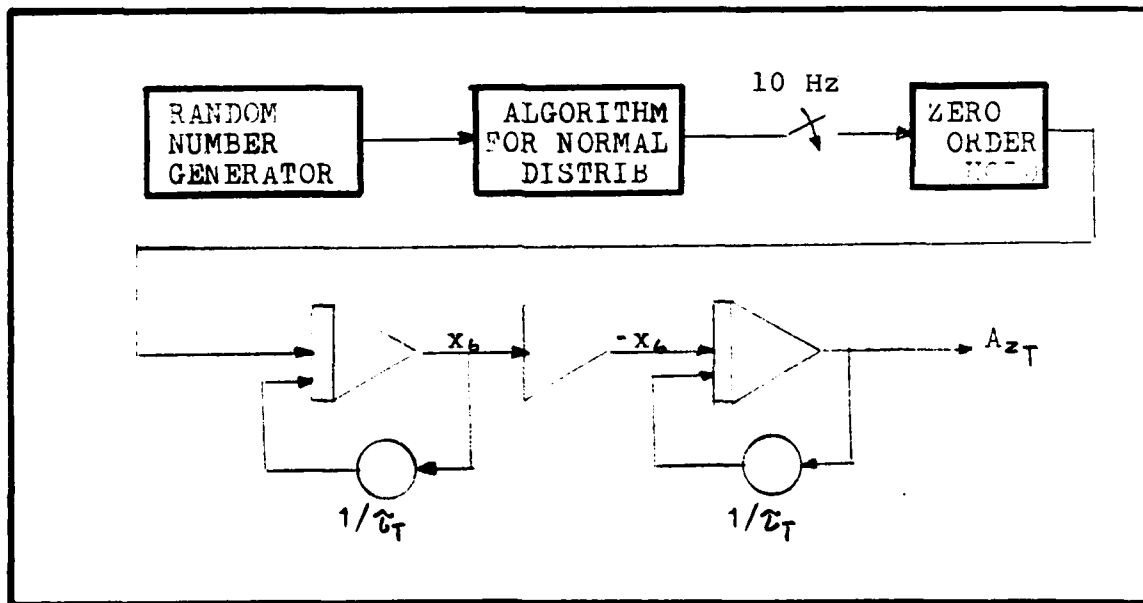


Figure 5. Filtered Input for Target Motion

that produced a white Gaussian distribution of random numbers with a mean of approximately zero and unit standard deviation. The standard deviation could be changed as required to provide the appropriate noise strength necessary to obtain the desired RMS value of  $A_{ZT}$ . A listing of the algorithm is contained in Appendix B.

The output of this Gaussian white noise generator was subjected to a double filter network to obtain a random function which represented "realistic" target motion. The same break frequency,  $1/\tau_T$ , used in Ref 1, was used in this study, i.e.  $\tau_T=3$  seconds. Figure 5 shows the analog schematic used to generate  $A_{ZT}$ .

#### Target Interface with the System

With the target acceleration,  $A_{ZT}$ , now available as an input, the expression for target flight path angle can be expressed as (Ref 6:298)

$$A_{ZT} = -\dot{\gamma}_T V_T \quad (28)$$

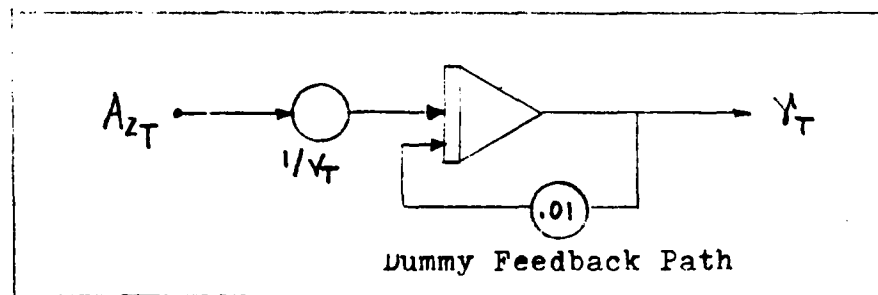


Figure 6. Analog Circuit for Target Flight Path Generation.

therefore

$$\dot{\gamma}_T = -\frac{1}{V_T} A_{Z_T} \quad (29)$$

Figure 6 is the analog schematic of target motion input to the system dynamics, specifically to the  $\dot{\gamma}_T$  and then the  $\dot{\Sigma}_T$  equations.

Though it does not appear in equation (29) a dummy feed-back path was added to the  $\dot{\gamma}_T$  equation to keep the steady state covariance of  $\gamma_T$  from becoming infinite (See Section IV). A nominal value of 0.01 was used in this feedback path so that it would have little, if any, effect on the actual dynamics being modelled.

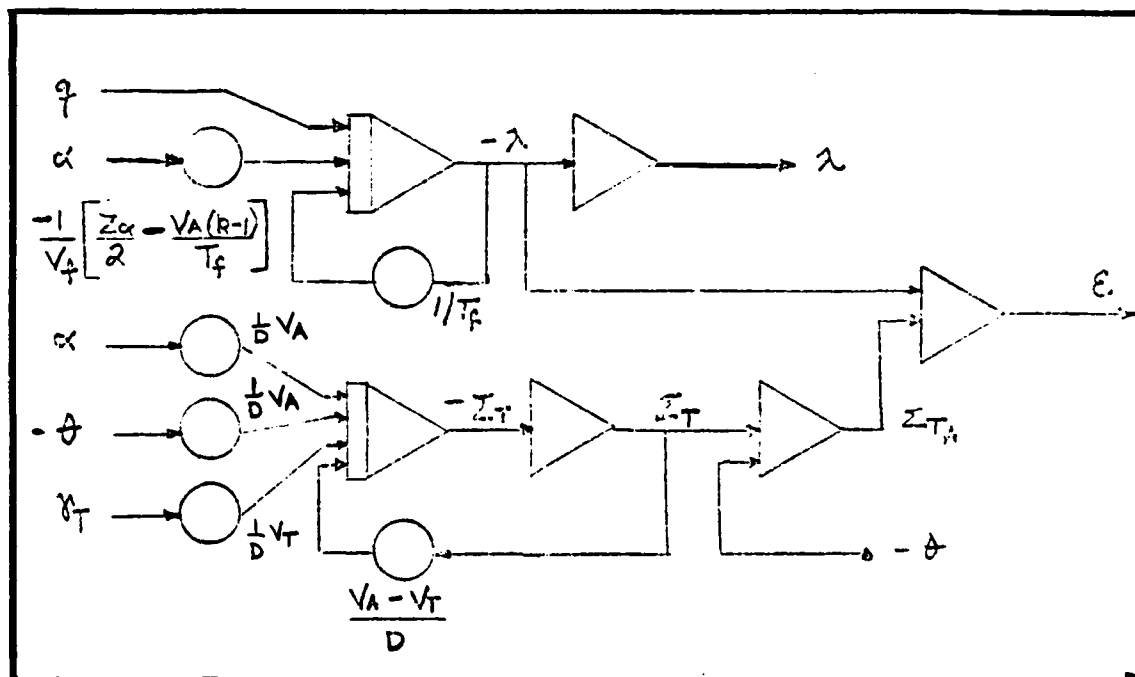


Figure 7. Analog Representation of Sight and Problem Kinematics

### Target Kinematics

The lead angle and line of sight angle equations were derived in Section II as equations (16) and (19) respectively. The analog models of these equations are shown in Figure 7. Also shown are the circuits for the computation of  $\Sigma_{TA}$ , the relative line of sight of the target with respect to the attacker weapon line, and  $\epsilon$ , the tracking error. The mathematical relationships for these last two parameters were derived from the geometry of Fig 2 as

$$\Sigma_{TA} = \theta - \Sigma_T$$

and

$$\epsilon = \lambda - \Sigma_{TA} \quad (30)$$

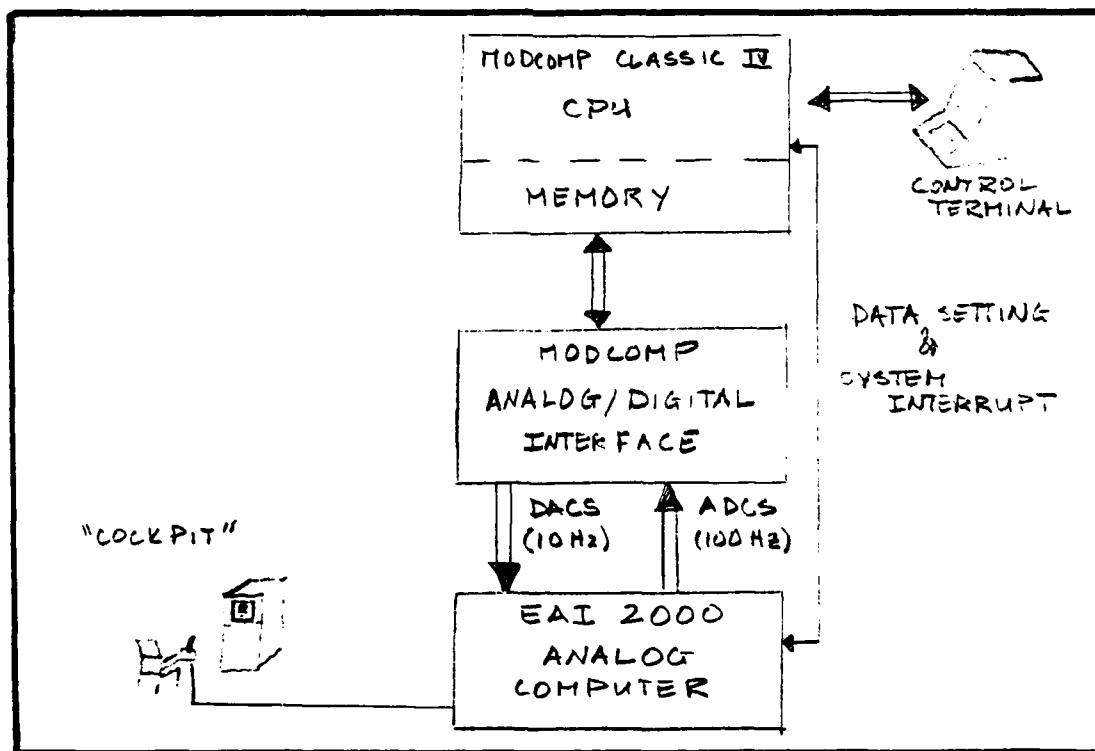


Figure 8. Functional Diagram of Hybrid Computer



### Hybrid Computer

The analog simulation was performed on the EAI 2000 Hybrid/MODCOMP Classic IV computer. Figure 8 shows a functional schematic of the system. A brief description of its operation follows.

The analog circuitry of the system model was installed on the EAI 2000 in usual fashion and connected to the MODCOMP Classic IV CPU through the analog/digital interface. Written in Classic FORTRAN IV, a driver program was entered via the interactive control terminal. In conjunction with the A/D interface and the operator at the control terminal, the computer performed the following functions: set the analog

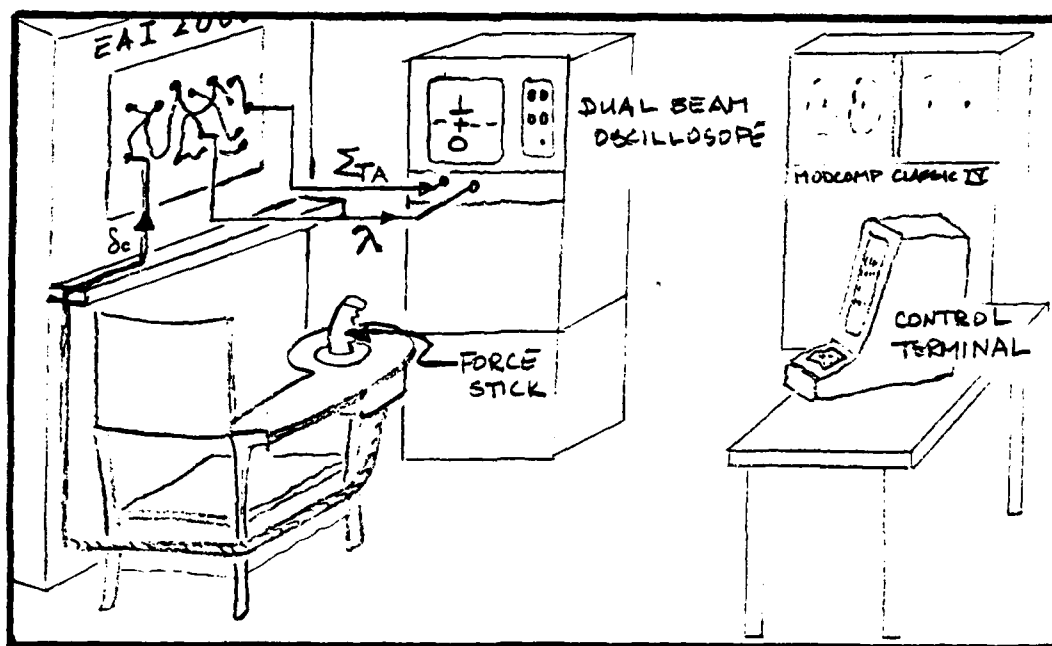


Figure 9. Depiction of Simulator Cockpit Equipment

potentiometers, triggered the simulation to start, provided the simulation with digital random noise (at 10Hz) as system input, signalled the A/D interface to sample and store in memory (at 100Hz) each of the states via the DACS (Digital to Analog Converters)/ADCS (Analog to Digital Converters), caused the system to interrupt at the end of the 10 second run time and finally processed the stored data for variance determination of each state for each run. The results were then printed on a line printer and at the control terminal.

#### Fixed Base Simulator

Figure 9 depicts the simulator "cockpit" used in this study. It consists of a student desk with side mounted control stick and a dual beam oscilloscope upon which the task

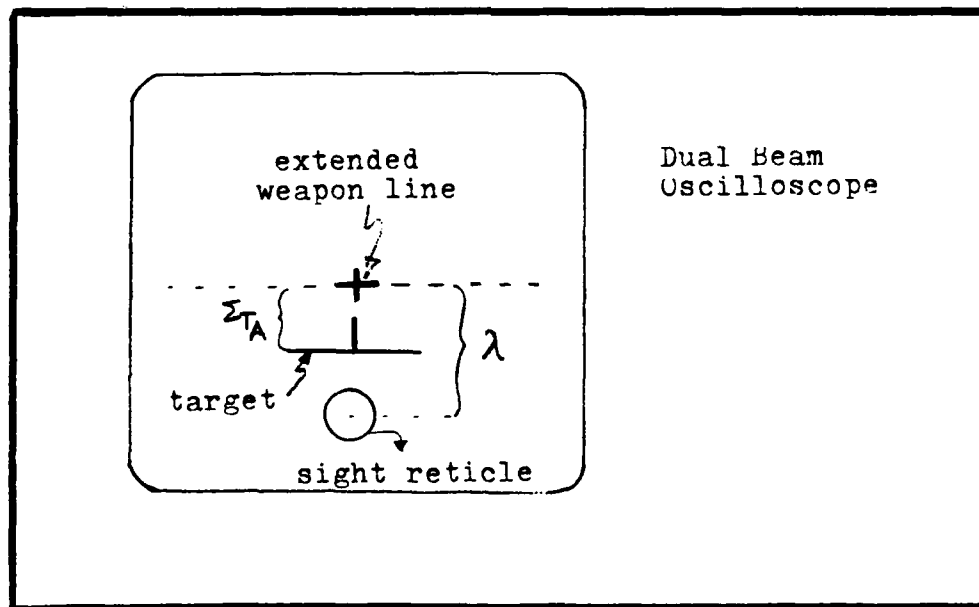


Figure 10. Simulation Display

was displayed at eye level. The side-stick controller is similar to those being used in light-weight fighter, fly-by-wire designs. In this simulation the stick was trimmed for level flight and could not be retrimmed.

Presentation of the Task to the Pilot. When tracking a target, the pilot of the pursuing aircraft is aware primarily of two parameters: the position of the target and the position of the sight. The difference between the two positions is the tracking error, and this is what the pilot attempts to minimize. In this simulation, the target is displayed on the oscilloscope, the center of which was assumed to be the extension of the aircraft's weapon line. The target is depressed below the weapon line by the current magnitude of  $\Sigma_{TA}$ , the relative line of sight to the target. The sight is positioned relative to the center of the oscilloscope by the current magnitude of  $\lambda$ , the lead angle. Figure 10 illustrates the picture seen by the pilot. The tracking error shown is positive; i.e., the attacker is lagging behind the target. Note that only the reticle portion of the sight is represented. This is due to the limitations encountered on being able to physically generate both the reticle and the pipper, as well as the target symbol, on the same oscilloscope at the same time. The pilots thus had to estimate the position of the center of the reticle to achieve zero-error tracking.

The Gathering of Data. After an extended period of training during which the three pilots became used to the task before them and the feel of the side-mounted, force-stick controller, the taking of data began. Twelve separate cases were run using three different aircraft dynamics, two ranges, and target RMS G levels of 3.5G's and 5.0G's. The three aircraft were the F-4E, the F-5, and the A-7. A summary of the dynamics of each aircraft is presented in (Ref 1:27) Table I. Ranges of 3000 feet and 1000 feet were decided upon since they represent approximate maximum and minimum tracking ranges in an actual situation. Five different target motions of either 3.5G or 5.0G RMS normal acceleration were run for each of the 12 cases. Thus each pilot flew a minimum of 60 times after data gathering runs began. A tracking time of 10 seconds was selected to represent the short term task.

A typical data run began with the target and the sight both stationary in the center of the screen, making all initial conditions equal to zero. The picture thus displayed represented a situation in which, unbeknown to the target, the attacker had maneuvered into a stern, or "6 o'clock", attack position. When the pilot was ready, the computer operator, through commands at the control terminal, initiated target motion to simulate high "G" evasive action whereupon the pilot began to track the target on the display screen

Table I  
Dynamic Parameters and Stability Derivatives

Aircraft	F-4E	F-5	A-7
Altitude (Ft)	15,000	5,135	15,000
Mach Number	0.90	0.81	0.60
Velocity, V (Ft/Sec)	951.6	889.0	635.0
Dynamic Pressure, q (Lb/Ft)	677.3	804.4	301.0
Mass, m (Slugs)	1433.5	354.0	680.0
Reference Area, S (Ft)	530.0	170.0	375.0
$Z_{\alpha}$ (Ft/Sec <sup>2</sup> )	-982.6	-1525.9	-730.4
$Z_{\delta}$ (Ft/Sec <sup>2</sup> )	-90.5	-331.9	-99.6
$M_{\alpha}$ (1/Sec <sup>2</sup> )	-10.443	-10.30	-9.08
$M_{\alpha}^*$ (1/Sec)	-0.3439	-0.0646	-0.133
$M_q$ (1/Sec)	-0.7381	-1.350	-0.696
$M_{\delta}$ (1/Sec <sup>2</sup> )	-37.08	-47.2	-18.90
$\omega_n$ (rad/sec)	3.35	3.88	3.00
$\zeta$ (-)	0.32	0.40	0.21

with input from the stick controller. At the same time the hybrid computer commenced taking data samples, at the rate of 100 per second for the next 10 seconds. The variables sampled were elevator deflection,  $\delta$ , pitch rate,  $q$ , lead angle,  $\lambda$ , relative line of sight angle of the target,  $\Sigma_{TA}$ , tracking error,  $\epsilon$ , and normal acceleration,  $A_{Z_T}$ . Figure 11

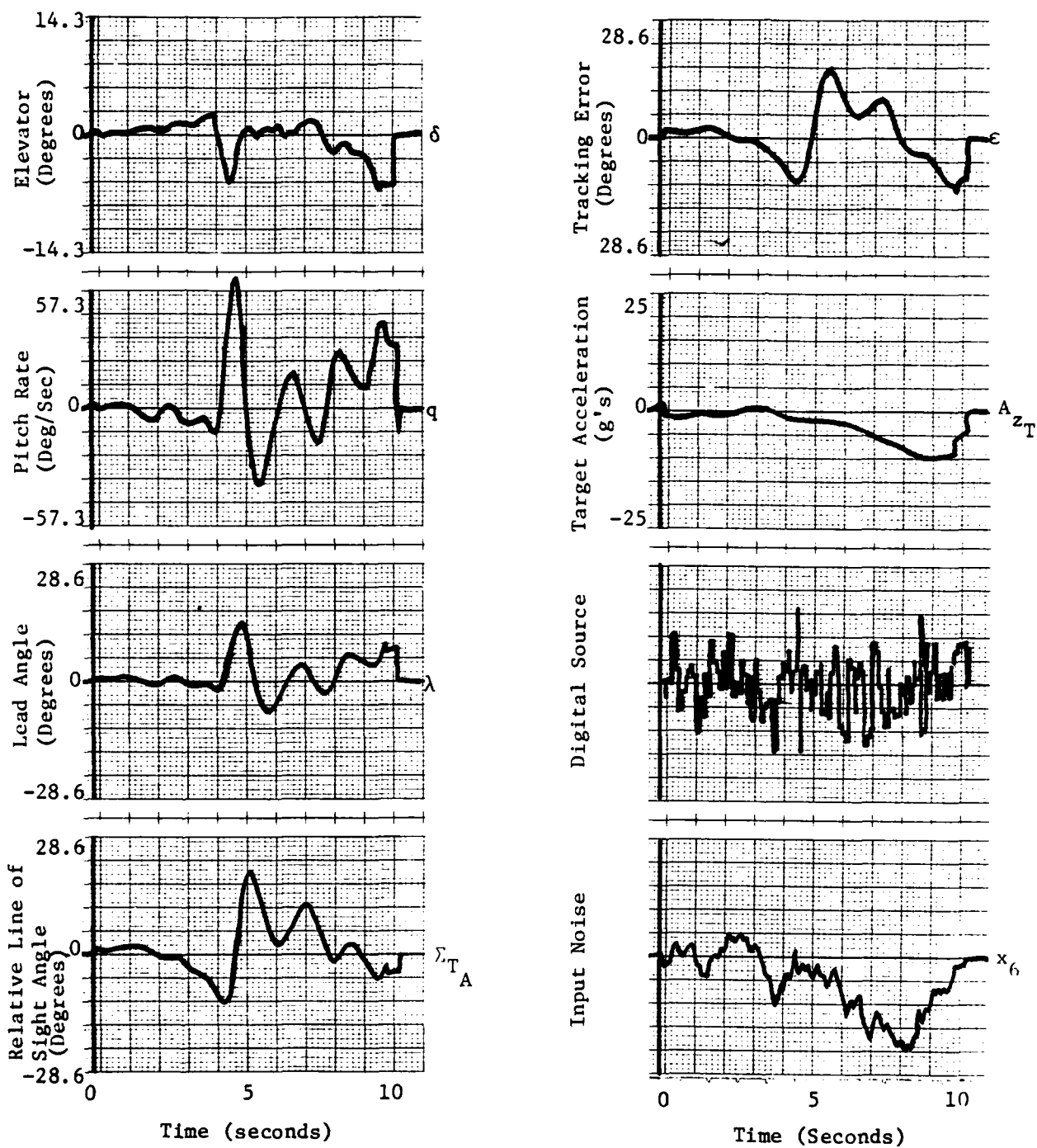


Figure 11. Plots of Typical Tracking Performance of Input and Recorded Variables (F4E - 1000 ft/3.5g)

shows the tracking performance of a typical run.

### Data Reduction

Since the target motion is filtered Gaussian white noise and the system is linear, the statistics of the system states are assumed to be stationary and ergodic. The mean and auto-correlation functions can be approximated by (Ref 6:580)

$$E\{X\} = \frac{1}{T} \int_0^T X \, dt$$

$$E\{X^2\} = \frac{1}{T} \int_0^T X^2 \, dt$$

Actual determination of the variance was accomplished digitally using the standard formula for variance (Ref 9:130)

$$\sigma^2 = \frac{1}{N} \sum_{i=1}^N X_i^2 - \left( \frac{1}{N} \sum_{i=1}^N X_i \right)^2 \quad (31)$$

The variables were sampled 100 times per second so that after each 10 second run, the standard deviation of each recorded variable was computed from the 1000 samples of stored data as square root of  $\sigma^2$  from (31). Once the 5 runs for each of the 12 cases was completed an average standard deviation was computed and recorded.

The complete tabulated results of the hybrid simulation are attached to this report as Appendix C. A discussion of the results is contained in Section V. A summary of the

flying experience of the pilots who flew the simulation is included as Appendix D.



#### IV. Analytic Solution Using an Optimal Model of the Human Controller

As stated initially this study attempts to determine whether the Optimal Pilot Model technique, used successfully by Harvey in Ref 1 to predict pilot performance for long term tracking tasks, can be used to predict pilot performance for short term tracking tasks.

The OPM is based upon optimal stochastic control theory and was initially developed by Kleinman, Baron, and Levison using the assumption that a "well-trained human operator behaves in an optimal manner for the given control task subject to his inherent limitations and constraints" (Ref 2:358). To perform the analysis required for this study, use was made of the OPM assembled by Enright (Ref 5) which was based on the theory of Kleinman et al. above. An overview of this model follows.

##### The Optimal Pilot Model

An Overview. Figure 12 is a functional description of the optimal pilot model and its interface with the system dynamics. It evolves from the optimal control system through inclusion of limitation features that model the inherent observation time delay, the neuromotor dynamics and the controller remnant associated with a human controller.

The observation time delays are those associated with relaying and processing visual information to the brain and

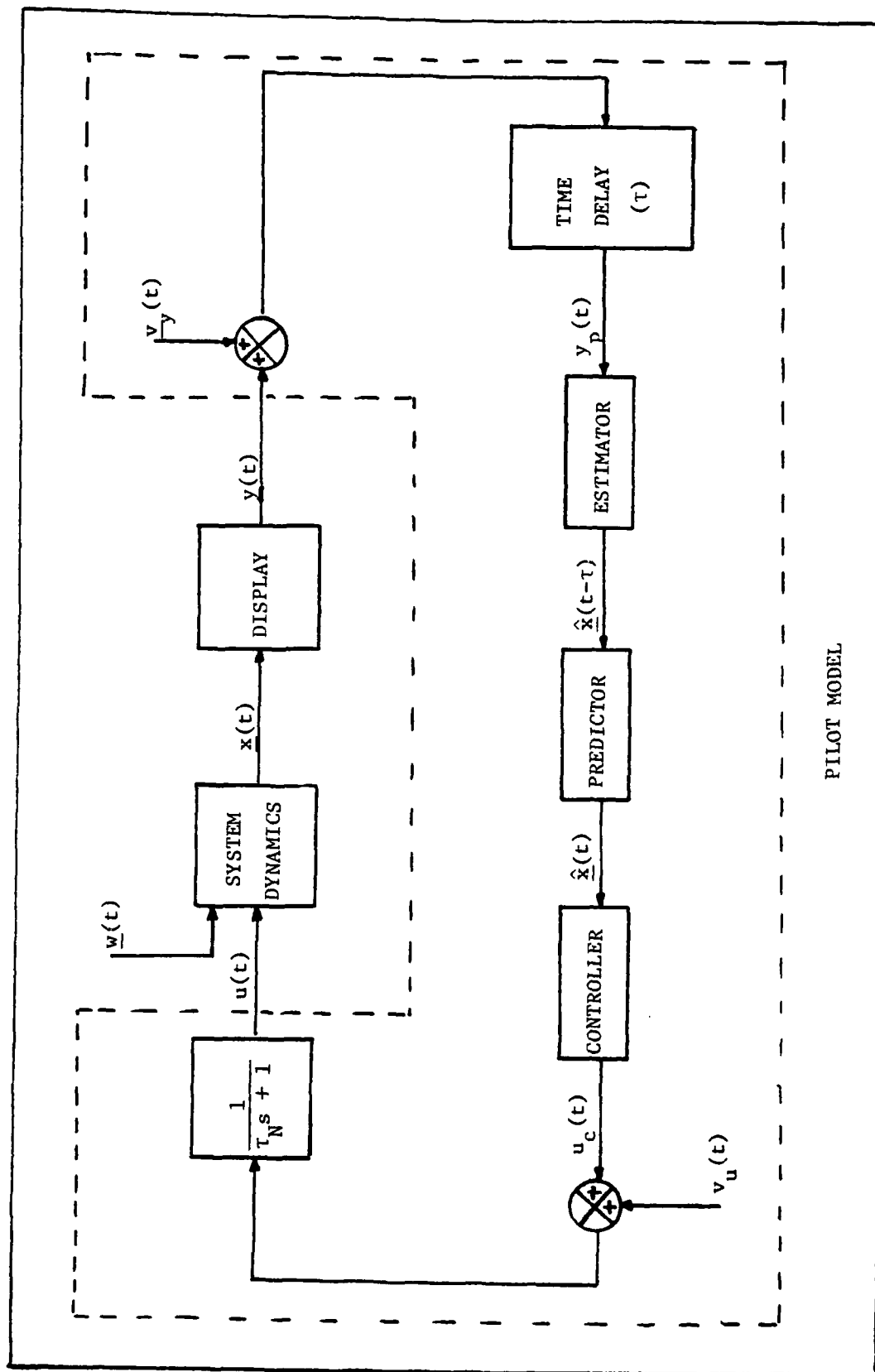


Figure 12. Functional Schematic of the Optimal Pilot Model in the Control Loop

are modeled by lumping them into a single equivalent perceptual time delay,  $\tau$ , with typical values of  $\tau$  being  $0.2 \pm 0.05$  seconds (Ref 2:363). The pilot thus perceives

$$\underline{y}_p(t) = \underline{y}(t-\tau) + \underline{v}_y(t-\tau) \quad (32)$$

The neuromotor dynamics are modeled by including a first order lag of the form  $(\tau_N s + 1)^{-1}$  where  $\tau_N$  is the neuromuscular time delay. This accounts for the limitations on the pilot's ability, or reluctance, to make rapid or excessive control movements. Controller remnant is that component of human response that accounts for the inherent random errors associated with perception of displayed variables and in the execution of control movements. Since the model is linear these errors are lumped as observation noises,  $\underline{v}_y$  and motor noise,  $v_u$ . These  $\underline{v}_y$  and  $v_u$  are assumed independent, zero mean Gaussian noises of sufficient bandwidth as to be considered white noise processes with covariances

$$\begin{aligned} E\{\underline{v}_y(t) \underline{v}_y^T(\sigma)\} &= V_y \delta(t-\sigma) \\ E\{v_u(t) v_u(\sigma)\} &= V_u \delta(t-\sigma) \end{aligned} \quad (33)$$

This delayed, noisy observation is operated on by a Kalman estimator in cascade with a least mean square predictor to yield a "best estimate",  $\hat{\underline{x}}(t)$  of the state at time  $t$ , conditioned on the observed output  $\underline{y}_p(\sigma)$ ,  $\sigma \leq t$ . This estimate is

then weighted by a set of optimal feedback gains,  $-\underline{l}^*$ , to produce a commanded control input,  $u_c(t)$ . The optimal feedback gains are determined separately outside the control loop. Note that for this study, the control input,  $u(t)$  is a scalar.

Creating the Optimal Control. The original system model, assumed linear and time-invariant, is given by

$$\dot{\underline{x}}(t) = A\underline{x}(t) + \underline{b}u(t) + \underline{w}(t) \quad (34)$$

$$\underline{y}(t) = H\underline{x}(t) \quad (35)$$

where  $\underline{y}(t)$  is the vector of observed variables and  $\underline{w}(t)$  is a zero mean, Gaussian, white noise vector needed to model the random target motion. It has a covariance of

$$E\{\underline{w}(t)\underline{w}^T(\sigma)\} = W \delta(t-\sigma) \quad (36)$$

The function of the pilot model is to determine the control input  $u(t)$  that minimizes the quadratic cost functional  $J(u)$ , conditioned on the observation  $\underline{y}(t)$ . Addition of the first order lag  $(\tau_N S + 1)^{-1}$  has the same effect on the system as including a cost term on control rate,  $\dot{u}(t)$ . This yields

$$J(u) = \frac{1}{2} \int_0^\infty \{ \underline{x}^T Q_x \underline{x} + u^2 r + \dot{u}^2 g \} dt \quad (37)$$

where  $Q_x$  is a symmetric, positive semi-definite weighting matrix. The scalar  $r$  is a non-negative weighting on  $u(t)$  while  $g$  is a positive weighting on  $\dot{u}(t)$ . To include the  $\dot{u}^2 g$  term to  $J(u)$  it is necessary to include  $\dot{u}(t)$  as the

(n+1) state variable.

Although required for modelling the pilot neuromuscular lag, the simple insertion of  $(\tau_N s + 1)^{-1}$  into the system would cause the input from the optimal pilot to the aircraft to be calculated incorrectly. The correct procedure, as shown in detail in Ref 2 (pg. 10-15), is to provide the system with an effective first order lag by inserting an integrator with feedback of the (n+1) state,  $u(t)$ , as shown in Fig 13a. This creates the augmented open loop system

$$\dot{\underline{z}} = \underline{A}_0 \underline{z} + \underline{b}_0 u \quad (38)$$

where

$$\underline{z} = \begin{bmatrix} \underline{x} \\ \underline{u} \end{bmatrix} \quad \underline{A}_0 = \begin{bmatrix} \underline{A} & \underline{b} \\ 0 & 0 \end{bmatrix} \quad \underline{b}_0 = \begin{bmatrix} 0 \\ 1 \end{bmatrix} \quad (39)$$

The cost functional then becomes

$$\begin{aligned} J(u) &= \frac{1}{2} \int_0^\infty \{ \underline{z}^T \underline{Q}_0 \underline{z} + u^2 g \} dt \\ &= \frac{1}{2} \int_0^\infty \{ [\underline{x}^T, u] \begin{bmatrix} \underline{Q}_x & 0 \\ 0 & r \end{bmatrix} \begin{bmatrix} \underline{x} \\ u \end{bmatrix} + u^2 g \} dt \end{aligned} \quad (40)$$

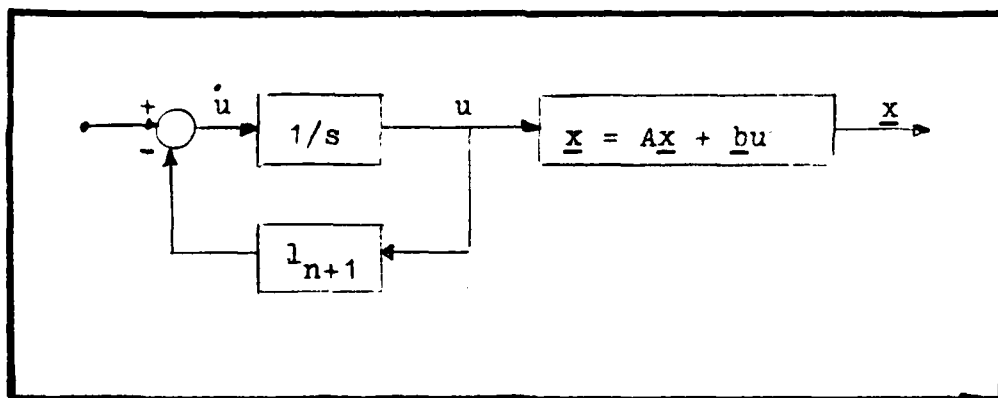


Figure 13a. Equivalent First Order Lag Included to Model Neuromuscular Delay

The optimal feedback gains are thus given by

$$\begin{aligned}\mu^* &= -[\underline{1}, \underline{1}_{n+1}] \underline{z} \\ &= -[g^{-1} \underline{b}_o^T K_o] \underline{z}\end{aligned}\quad (41)$$

where  $K_o$  is the unique positive definite solution to the  $n+1$  dimensional Riccati equation

$$A_o^T K_o + K_o A_o + Q_o - K_o \underline{b}_o \underline{b}_o^T K_o / g = 0 \quad (42)$$

and  $Q_o$  is the augmented state weighting matrix

$$Q_o = \begin{bmatrix} Q_x & 0 \\ 0 & r \end{bmatrix} \quad (43)$$

The resulting closed loop system can then be shown as in Fig 13b.

Reducing the integrator and  $\underline{1}_{n+1}$  feedback gives

$$\frac{\underline{u}}{\underline{u}_c} = \frac{1}{s + \underline{1}_{n+1}} = \frac{1/\underline{1}_{n+1}}{\frac{s}{\underline{1}_{n+1}} + 1} = \frac{\tau_N}{\tau_N s + 1} \quad (44)$$

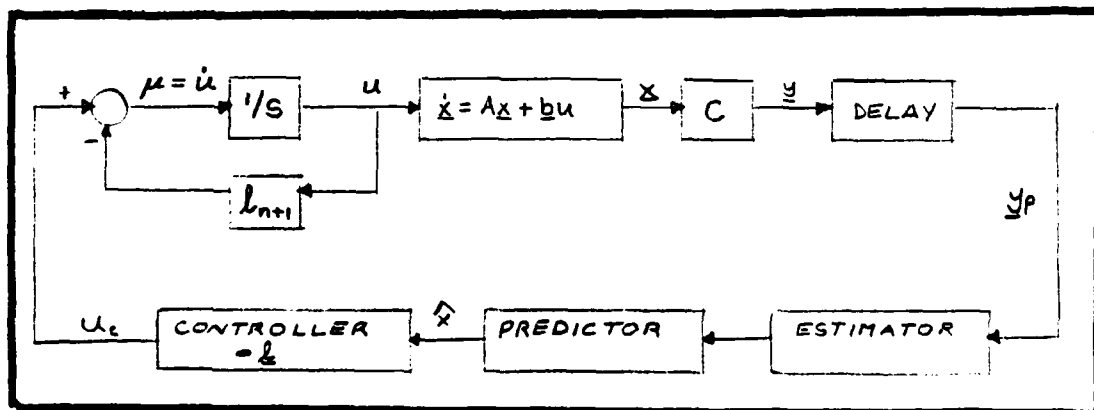


Figure 13b. Optimal Pilot Model (Closed Loop) with Equivalent Neuromuscular Lag Included

where  $\tau_N$  has been defined as  $1/l_{n+1}$ . Thus a further equivalent closed loop system is obtained with the first order lag included as previously proposed. By moving the  $\tau_N$  factor to the controller gain and adding the input noise, observation noise and motor noise, one obtains Fig 13c from which it can be seen, that

$$\tau_N \dot{u}(t) + u(t) = u_c(t) + v_u(t) = -\underline{l}^* \hat{x} + v_u(t) \quad (45)$$

Thus

$$u_c(t) = -\underline{l}^* \hat{x} \quad (46)$$

and

$$l_i^* = \tau_N l_i, \quad i = 1, 2, \dots, n \quad (47)$$

The  $(n+1)$ th state equation becomes

$$\dot{u}(t) = \frac{-1}{\tau_N} u(t) + \frac{1}{\tau_N} u_c(t) + \frac{1}{\tau_N} v_u(t) \quad (48)$$

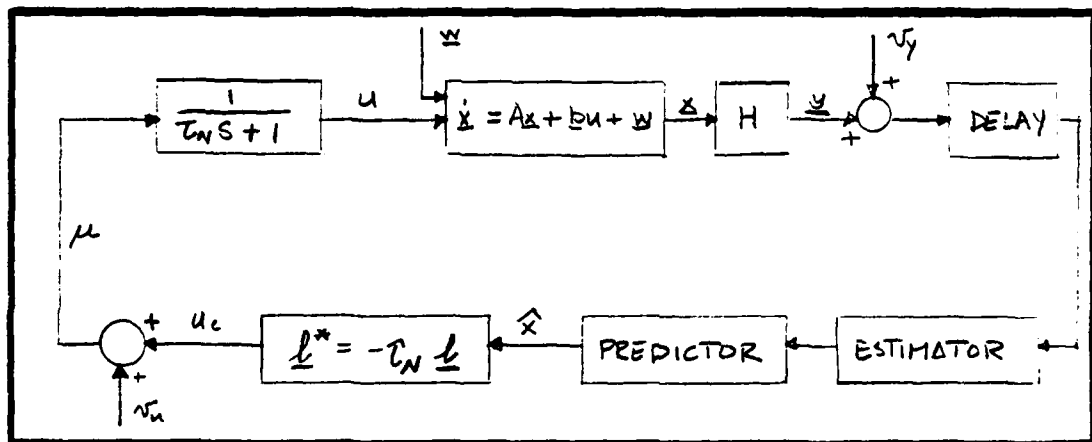


Figure 13c. Optimal Pilot Model (Closed Loop) with First Order Lag and Correct Form of Optimal Input

where  $u_c(t)$  is defined as the control input to the augmented system dynamics. The augmented system becomes

$$\begin{aligned}\dot{\underline{z}}(t) &= A_1 \underline{z}(t) + \underline{b}_1 u_c(t) + \underline{w}_1(t) \\ &= \begin{bmatrix} A & \underline{b} \\ \underline{0} & -1/\tau_N \end{bmatrix} \begin{bmatrix} \underline{x}(t) \\ u(t) \end{bmatrix} + \begin{bmatrix} \underline{0} \\ 1/\tau_N \end{bmatrix} u_c(t) + \begin{bmatrix} \underline{w}(t) \\ \frac{\dot{\underline{v}}_u(t)}{\tau_N} \end{bmatrix} \quad (49)\end{aligned}$$

with the covariance of  $\underline{w}_1(t)$  given by

$$E\{\underline{w}_1(t) \underline{w}_1^T(\sigma)\} = \begin{bmatrix} \underline{w} & \underline{0} \\ \underline{0} & \dot{\underline{v}}_u / \tau_N^2 \end{bmatrix} \delta(t-\sigma) \quad (50)$$

#### Optimal Estimator and Predictor

Two variables are displayed to the pilot in this study, the tracking error,  $\epsilon$ , and the relative LOS,  $\Sigma_{TA}$ . It is assumed also that he can perceive their first derivatives from this display. The output or observation vector is given by

$$\underline{y}(t) = H_1 \underline{z}(t) = [H:0] \begin{bmatrix} \underline{x} \\ u \end{bmatrix} \quad (51)$$

where  $H_1$  is the constant augmented observation matrix.

Due to remnant effects discussed earlier, the pilot actually perceives a delayed, noisy rendition of the true system output,

$$\underline{y}_p(t) = H_1 \underline{z}(t-\tau) + \underline{v}_y(t-\tau) \quad (52)$$

where  $\tau$ , the equivalent perceptual time delay of the model, defined earlier, was chosen as 0.2 seconds, the same value



as used in Ref 1.

From this perceived output the Kalman filter produces a least mean squared estimate  $\hat{\underline{z}}(t-\tau)$  of the delayed state  $\underline{z}(t-\tau)$  through the solution of the differential equation (Ref 9:217)

$$\begin{aligned} \dot{\hat{\underline{z}}}(t-\tau) = & A_1 \hat{\underline{z}}(t-\tau) + CH_1^T V_Y^{-1} [\underline{y}_p(t) - H_1 \hat{\underline{z}}(t-\tau)] \\ & + \underline{b}_1 u_c(t-\tau) \end{aligned} \quad (53)$$

where C, the error covariance matrix, satisfies the steady state Riccatti equation (Ref 2:362)

$$A_1 C + C A_1^T + W_1 - CH_1^T V_Y^{-1} H_1 C = 0 \quad (54)$$

The predictor then generates a current time estimate  $\hat{\underline{z}}(t) = \text{col}[\hat{\underline{x}}, \hat{\underline{u}}(t)]$  from

$$\hat{\underline{z}}(t) = e^{A_1 \tau} [\hat{\underline{z}}(t-\tau) - \underline{\zeta}(t-\tau)] + \underline{\zeta}(t) \quad (55)$$

where  $\underline{\zeta}(t)$  is generated by

$$\dot{\underline{\zeta}}(t) = A_1 \underline{\zeta}(t) + \underline{b}_1 u_c(t) \quad (56)$$

Figure 14 is a detailed diagram of the computational flow involved in this model. Notice that the noise input,  $\underline{w}_1(t)$ , to the system dynamics is now a combination of target driving noise,  $w(t)$ , and motor noise,  $v_u(t)$ , as given in equation (49). Also note that  $\underline{1}_1^*$  in the diagram is defined as the  $n+1$  dimension row vector  $[\underline{1}^*:0]$  where  $\underline{1}^*$  is given by equations (46) and (47).

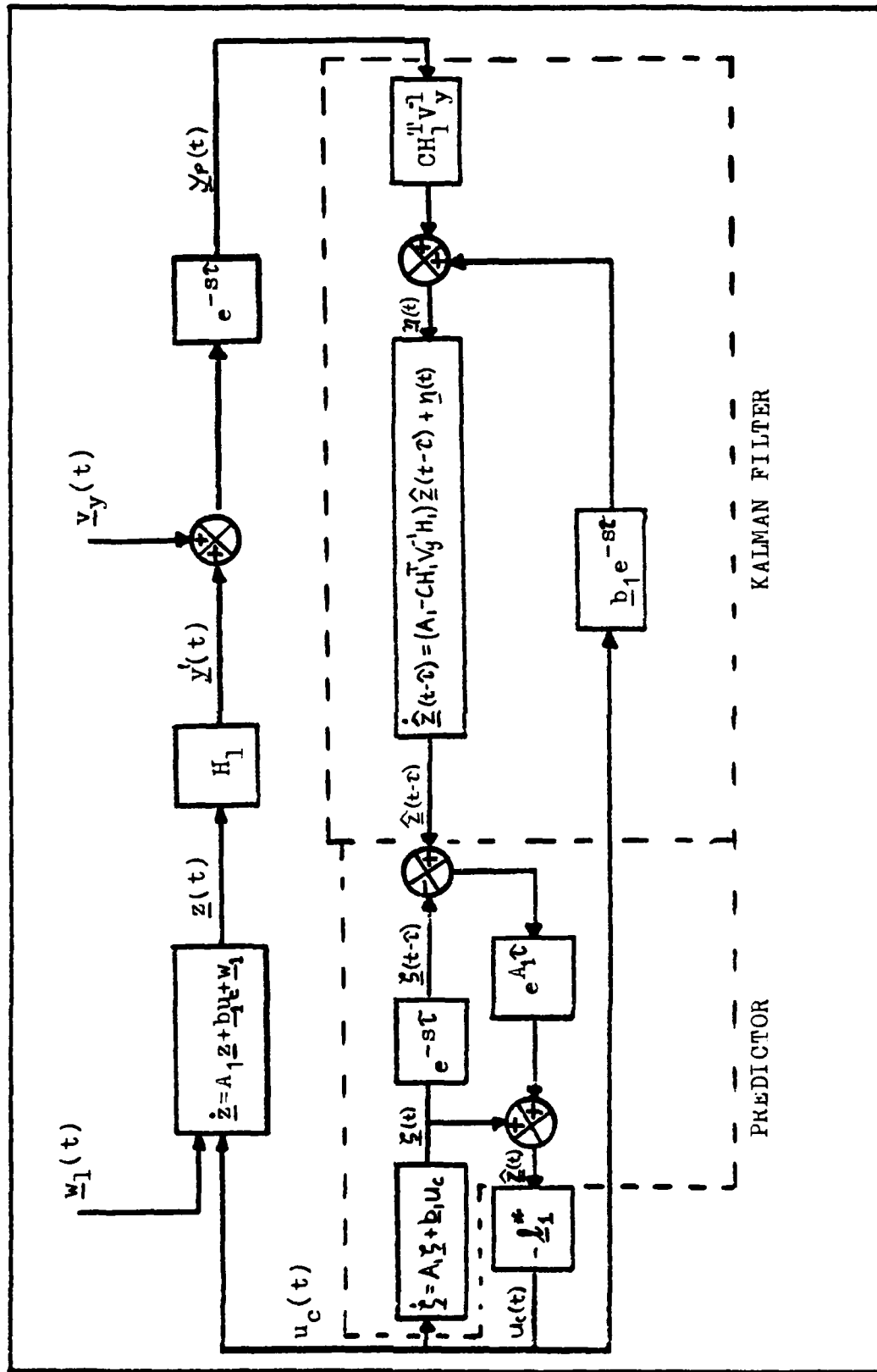


Figure 14. Computational Flow Diagram of the Optimal Pilot Model in the Control Loop (System Equations Augmented).

### System Statistics

The system states statistics are generated in the form of the covariance of  $\underline{z}(t)$  via the expression (Ref 2:363)

$$E\{\underline{z}(t)\underline{z}^T(t)\} = e^{\underline{A}_1 t} C e^{\underline{A}_1^T t} + \int_0^t e^{\underline{A}_1 \sigma} \underline{W}_1 e^{\underline{A}_1^T \sigma} d\sigma \\ + \int_0^\infty e^{\bar{\underline{A}} \sigma} \underline{A}_1^T C^T H_1^T V_Y^{-1} H_1 C e^{\underline{A}_1^T \tau} e^{\bar{\underline{A}}^T \sigma} d\sigma \quad (57)$$

where

$$\bar{\underline{A}} = \begin{bmatrix} \underline{A} & \vdots \\ -\underline{1}^*/\tau_N & -\underline{1}/\tau_N \end{bmatrix} \quad (58)$$

The solution to the third term in this equation can be easily obtained by noting that expressions of the form

$$\underline{X} = \int_0^\infty e^{\bar{\underline{A}} t} \underline{Y} e^{\underline{A}^T t} dt \quad (59)$$

can be evaluated from the solution to (Ref 9:143)

$$\underline{A}\underline{X} + \underline{X}\underline{A}^T + \underline{Y} = 0 \quad (60)$$

Further computational methods for evaluation of (57) are described in Ref 4. The standard deviations of the system states are then computed by taking the square root of the appropriate diagonal element of the state covariance matrix. Finally the output covariance matrix is computed from

$$E\{\underline{y}(t)\underline{y}^T(t)\} = H_1 E\{\underline{z}(t)\underline{z}^T(t)\} H_1^T \quad (61)$$

### Application to the Air-to-Air Task

The State Equations of Motion. The dynamic variables

describing the air-to-air task were listed in Section II. They are repeated here in state variable format, again the same used by Harvey:

$$\begin{aligned}
 x_1 &= \delta & x_6 &= \text{dummy state} \\
 x_2 &= q & x_7 &= A Z_T \\
 x_3 &= \alpha & x_8 &= \gamma_T \\
 x_4 &= \lambda & x_9 &= \theta \\
 x_5 &= \Sigma_T
 \end{aligned} \tag{62}$$

and

$$u \equiv \delta_c = -K_f F_s \tag{63}$$

Equations (25), (23), (21), (16), (19), (29), and (20) together with the target shaping filter equations are represented in the system dynamic notation

$$\dot{\underline{x}} = A\underline{x}(t) + B\underline{u}(t) + \underline{W}(t) \tag{64}$$

in which the "A" matrix is

$$\begin{bmatrix}
 -1/\tau_a & 0 & 0 & 0 & 0 & 0 & 0 & 0 & 0 \\
 \frac{(M_s + M_s Z_\delta)}{U_o} & \frac{(M_q + M_q)}{U_o} & \frac{(M_\alpha + M_\alpha Z_\alpha)}{U_o} & 0 & 0 & 0 & 0 & 0 & 0 \\
 Z_\delta/U_o & 1 & Z_\alpha/U_o & 0 & 0 & 0 & 0 & 0 & 0 \\
 0 & 1 & a_{43} & -1/T_f & 0 & 0 & 0 & 0 & 0 \\
 0 & 0 & V_A/D & 0 & \frac{V_A - V_T}{D} & 0 & 0 & V_T/D & -V_A/D \\
 0 & 0 & 0 & 0 & 0 & -1/\tau_T & 0 & 0 & 0 \\
 0 & 0 & 0 & 0 & 0 & 1 & -1/\tau_T & 0 & 0 \\
 0 & 0 & 0 & 0 & 0 & 0 & -1/V_T & -0.01^* & 0 \\
 0 & 1 & 0 & 0 & 0 & 0 & 0 & 0 & 0
 \end{bmatrix}$$

where

$$a_{43} = -\frac{1}{V_f} \left[ \frac{Z_\alpha}{2} - \frac{V_A(k-1)}{T_f} \right]$$

-----  
 + This term was zero in Ref 1 but to obtain convergent Riccati solution, was set to -0.005 in this study.

\* Dummy feedback on this state to insure finite covariance of  $\gamma_T$ .

Also,

$$\underline{b} = \text{col} [K_L/\tau_a \ 0 \ 0 \ 0 \ 0 \ 0 \ 0 \ 0 \ 0]$$

$$\underline{w}(t) = \text{col} [0 \ 0 \ 0 \ 0 \ 0 \ w \ 0 \ 0 \ 0] \quad (65)$$

where

$w$  = white, Gaussian driving noise.

From the display the pilot can extract the computed lead angle  $\lambda$ , the relative line of sight to the target  $\Sigma_{TA}$ , and tracking error  $\epsilon$ , plus the rates of change of each of the quantities. Since  $\Sigma_{TA}$ ,  $\lambda$ , and  $\epsilon$  are linearly dependent, only two of them need be represented in the observation vector  $\underline{y}(t)$ . The error and line of sight were used along with their respective rates because it was judged that the pilot was more aware of these quantities than of the lead angle. Thus the display is modelled by

$$\underline{y}(t) = H \underline{x}(t) \quad (66)$$

with

$$\underline{y}(t) = \text{col} [\epsilon \ \dot{\epsilon} \ \Sigma_{TA} \ \dot{\Sigma}_{TA}] \quad (67)$$

and the output or observation matrix H given by

$$\begin{bmatrix} 0 & 0 & 0 & 1 & 1 & 0 & 0 & 0 & 0 \\ 0 & 0 & h_{23} & -1/T_f & \frac{V_A - V_T}{D} & 0 & 0 & \frac{V_T}{D} & \frac{-V_A}{D} \\ 0 & 0 & 0 & 0 & -1 & 0 & 0 & 0 & 1 \\ 0 & 1 & \frac{-V_A}{D} & 0 & \frac{V_T - V_A}{D} & 0 & 0 & \frac{-V_T}{D} & \frac{V_A}{D} \end{bmatrix}$$

where

$$h_{23} = \frac{V_A}{D} - \frac{1}{V_f} \left[ \frac{Z_\alpha}{2} - \frac{V_A}{T_f} (k-1) \right] \quad (68)$$

The system statistics are obtained from the covariance of  $\underline{z}(t)$  which is determined from solution of equation (57). This requires apriori determination of certain noise covariances and threshold effects. Their determination follows.

#### Determination of Noise Covariances

Observation and motor noises depend upon the quality of the display, distraction related to the environment and human randomness so determination of numerical values for their covariances,  $V_y$  and  $V_u$  respectively, can be quite difficult. It has been found however that each white observation noise  $v_{y_i}(t)$  has a covariance that is related to the variance of its associated variable  $y_i$  by (Ref 2:363)

$$v_{y_i} = \pi \rho_i E\{y_i^2\} \quad (69)$$

where on the average  $\rho_i = 0.01$  which was used herein.

Similarly the motor noise covariance is assumed to be related to the variance of the commanded control,  $u_c(t)$  by (Ref 2:363)

$$v_u = \pi \rho_u E\{u_c^2\} \quad (70)$$

where typical value for  $\rho_u = 0.003$  which was used here also.

### Modelling Threshold Effects

In any visual task there exists a limit on the minimum arc of resolution that a controller can visually perceive. Additionally there are those errors detectable to the controller but smaller than his indifference threshold; errors he chooses to ignore.

In the pilot model for this task these effects are not distinguished and are modelled as a statistical linearization of the "deadzone" nonlinearity,  $f(y)$ , as shown in Fig. 15 where

$$f(y) = \begin{cases} y-a, & y \geq a \\ 0, & -a < y < a \\ y+a, & y \leq -a \end{cases} \quad (71)$$

Thus the controller perceives

$$y_{p1}(t) = f(y) + v_y(t) \quad (72)$$

In order to incorporate this threshold effect into the pilot model a linear representation of  $f(y)$  is needed. Such a representation can be developed (Ref 10:236-238) by using a difference function,  $d(t)$  where

$$d(t) = f(y) - \hat{f} \cdot y(t) \quad (73)$$

where  $\hat{f}$  is the linear approximation of  $f(y)$  and minimizes the relation

$$\begin{aligned} T &= E\{d^2(t)\} = E\{[f(y) - \hat{f} \cdot y(t)]^2\} \\ &= E\{[f(y)]^2 - 2\hat{f} \cdot y(t)[f(y)] + \hat{f}^2 \cdot y^2(t)\} \end{aligned} \quad (74)$$

To minimize  $T$ , equation 75 must be true

$$\frac{\partial T}{\partial \hat{f}} = 0 = E\{[0] - 2y(t) f(y) + 2[\hat{f} \cdot y^2(t)]\} \quad (75)$$

Thus

$$\begin{aligned} \hat{f} &= E\{y(t)f(y)\} [E\{y^2(t)\}]^{-1} \\ &= [\int_{-\infty}^{\infty} y(t) f(y) p(y) dy] / \sigma^2 \end{aligned} \quad (76)$$

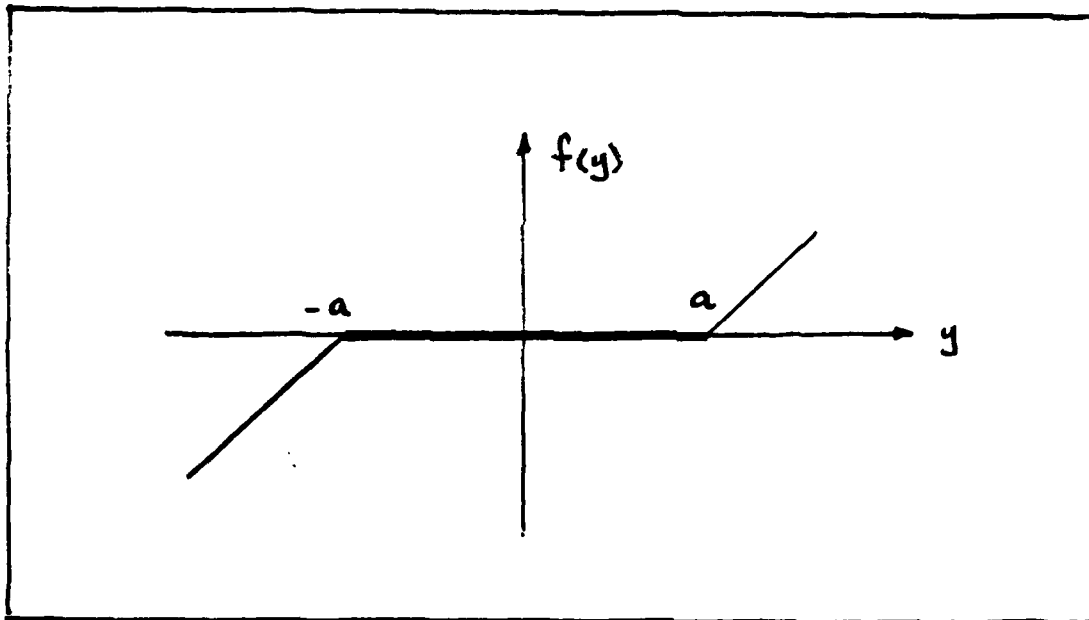


Figure 15. Plot of Threshold Nonlinearity



Since  $y(t)$  is assumed to be a Gaussian random variable with zero mean, then

$$\begin{aligned} p(y) &= \text{probability density function of } y \\ &= \frac{1}{\sqrt{2\pi}\sigma} \exp \left[ -\frac{1}{2} (y/\sigma)^2 \right] \end{aligned} \quad (77)$$

where  $\sigma$  is the standard deviation of  $y$ . Substituting  $p(y)$  into equation (76) and letting  $w = y/\sqrt{2}\sigma$ ,  $\hat{f}$  becomes

$$\begin{aligned} \hat{f} &= \frac{2}{\pi} \int_{-\infty}^{\infty} \frac{a}{\sigma\sqrt{2}} e^{-w^2} dw = 1 - \operatorname{erf}(a/\sigma\sqrt{2}) \\ &= \operatorname{erfc}(a/\sigma\sqrt{2}) \end{aligned} \quad (78)$$

where  $\operatorname{erfc}(a/\sigma\sqrt{2})$  is the complimentary error function of  $(a/\sqrt{2}\sigma)$ . Figure 16 shows how  $\hat{f}$  varies as the threshold,  $a$ , increases.

Equation (72) becomes

$$y_{p1}(t) \approx y_{p2}(t) = \hat{f} \cdot y(t) + v_y(t) \quad (79)$$

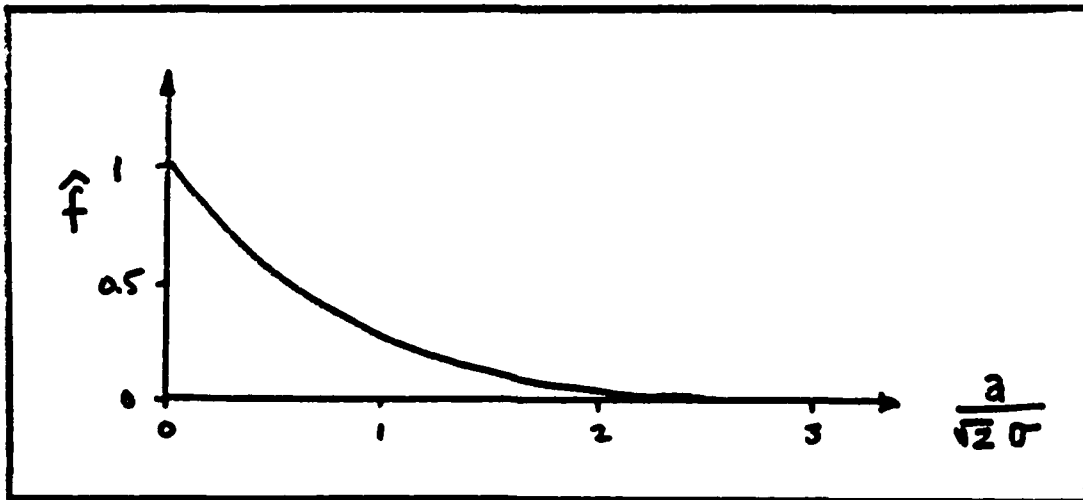


Figure 16. Plot of Threshold Nonlinearity Equivalent Gain,  $\hat{f}$

Since the pilot will mentally correct for this threshold, the measure he uses is

$$y_{p_3}(t) \equiv \frac{y_{p_2}(t)}{\hat{f}} = y(t) + \frac{v_y(t)}{\hat{f}} \quad (80)$$

so that the covariance of each observation noise becomes

$$v_{y_i} = \pi \rho_i \hat{f}_i^{-2} E\{y_i^2\} \quad (81)$$

It remains to determine the values for observation threshold, a.

It has been found that a  $\theta_{\min}$  of  $0.05^\circ$  is the typical minimum arc that a human controller can resolve (Ref 11:93). In this simulation 100 cm separated the observer from the display so  $0.05^\circ$  converts to approximately 0.087 cm on the oscilloscope screen. The screen display scaling for  $\epsilon$ ,  $S_\epsilon$ , was set at 9.5 deg/cm screen (.167 rad/cm). Therefore the

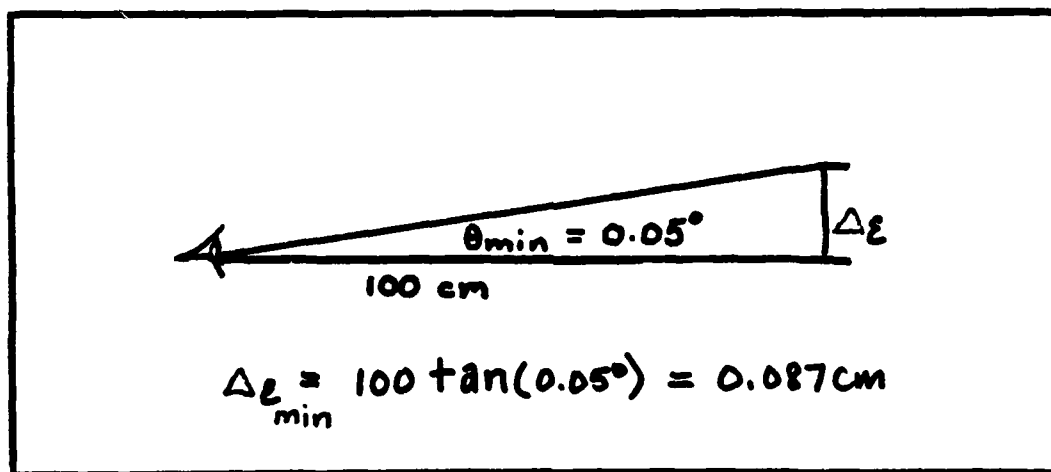


Figure 17. Visual Threshold Geometry

error threshold,  $a_\epsilon$ , was computed to be

$$a_\epsilon = \theta_{\min} S_\epsilon = 0.0146 \text{ rad} \quad (82)$$

Typical values for rate threshold are 0.05 to 0.1 degrees of visual arc per sec. Using the upper value for the error rate threshold gives  $a_\epsilon$  of 0.0295 rad/sec. Since the pilot obtains the relative line of sight angle,  $\Sigma_{TA}$  and its rate  $\dot{\Sigma}_{TA}$  from the same display, it was assumed similar thresholds applied.

#### Target Motion Noise Covariance, W

Determination of the target motion noise covariance W is accomplished using steady state covariance analysis. First consider the state equations for the target motion noise filters given by

$$\begin{aligned} \dot{x}_6 &= -\frac{1}{\tau_T} x_6 + w(t) \\ \dot{x}_7 &= x_6 - \frac{1}{\tau_T} x_7 \end{aligned} \quad (83)$$

or

$$\dot{\underline{x}} = A' \underline{x}' + \underline{w}' \quad (84)$$

where

$$A' = \begin{bmatrix} -1/\tau_T & 0 \\ 1 & -1/\tau_T \end{bmatrix} \quad \underline{x}' = \begin{bmatrix} x_6 \\ x_7 \end{bmatrix}$$

and

$$\underline{w}'(t) = \begin{bmatrix} w(t) \\ 0 \end{bmatrix} \quad (85)$$

Note that the primes indicate submatrices not the transpose.

The covariance of  $\underline{w}'(t)$  is given by

$$E[\underline{w}'(t) \underline{w}'^T(\sigma)] = W' \delta(t-\sigma) \quad (86)$$

The steady state covariance matrix  $P$  of  $\underline{x}'(t)$  is determined from solution of the linear steady state stochastic differential equation (Ref 9:167)

$$0 = A'P' + P'A'^T + W' \quad (87)$$

resulting in

$$P = E\{\underline{x}'(t) \underline{x}'^T(t)\} \\ = \begin{bmatrix} p_{66} & p_{67} \\ p_{76} & p_{77} \end{bmatrix} \quad (88)$$

where

$$p_{66} = \sigma_{x_6}^2 = \text{variance of } x_6(t) \\ p_{77} = \sigma_{x_7}^2 = \text{variance of } x_7(t) \quad (89) \\ p_{67} = p_{76} = E[x_6(t) x_7(t)]$$

Since the variance of  $x_7$  is the square of the target accelerations stipulated in the simulation, i.e. either 3.5G or 5.0G, equation (87) solves to give

$$W' = \begin{bmatrix} 4\sigma_{a_T}^2 & 0 \\ \frac{\tau^3}{T} & 0 \\ 0 & 0 \end{bmatrix} \quad (90)$$

#### Cost Functional Weightings, $Q_x$ , $r$ , $g$

The values of the individual terms of the cost functional

weighting matrices are usually chosen to vary inversely with the square of the maximum excursion anticipated for each of the respective state variables and control inputs. For example, to minimize the excursion of system state  $x_1$  to some value  $x_{1\max}$  a first guess for  $Q_x(1,1)$  might be  $1/x_{1\max}^2$ . If however system performance is based on the excursions made by the components of the output or observation vector,  $\underline{y}_p(t)$ , which in this study contains none of the system states directly, it becomes more meaningful to specify a weighting matrix,  $Q_y$ , for the observation states.

Since  $\underline{y}$  is linear combination of  $\underline{x}$  as given by

$$\underline{y} = H\underline{x} \quad (91)$$

it is possible to provide to the cost functional,  $J(u)$ , an equivalent  $Q_x$  that represents the considerations made on  $\underline{y}_p(t)$ . This is done by specifying a  $Q_y$  so that the actual cost functional term for  $\underline{x}$ , considered relative to the observation vector  $\underline{y}_p(t)$ , is

$$\begin{aligned} \underline{y}^T Q_y \underline{y} &= (H\underline{x})^T Q_y (H\underline{x}) \\ &= \underline{x}^T [H^T Q_y H] \underline{x} \\ &= \underline{x}^T [Q_x] \underline{x} \end{aligned} \quad (92)$$

Hence  $Q_x$  is obtained via the matrix transformation

$$Q_x = H^T Q_y H \quad (93)$$

As a starting point for this study, the final weighting matrices used by Harvey at Ref 1 were implemented. This provided a method to check that the optimal controller used in this study would replicate the results obtained in Ref 1.

Specifically, this set the weighting,  $r$ , on system control to zero, signifying that control input would not be penalized in the tracking task; the pilot was free to command as much elevator as possible to track the target. The weighting,  $g$ , on control rate was adjusted so the desired neuromotor lag time constant,  $\tau_N$ , was produced. This is due to the relationship between  $\tau_N$  and  $l_{n+1}$  given by equation (47) and the fact that the solution to the Riccati equation (42) relies upon a knowledge of  $g$ . Harvey used  $\tau_N = 0.1$  seconds which is typical (Ref 2:363).

The  $Q_y$  matrix used in this study requires some explanation. Harvey's final results were actually obtained using an observation vector  $\underline{y}'_p(t)$ , different from the original  $\underline{y}_p(t) = [\epsilon \dot{\epsilon} \Sigma_{TA} \dot{\Sigma}_{TA}]^T$ . He considered as the observation vector

$$\underline{y}'_p(t) = \begin{bmatrix} \epsilon \\ \dot{\epsilon} \\ \lambda \\ \epsilon \end{bmatrix} \quad (94)$$

where  $\underline{y}'_p(t)$  is obtained from  $\underline{y}_p(t)$  by

$$\begin{aligned} \underline{y}'_p(t) &= H' \underline{y}_p(t) \\ &= \begin{bmatrix} 1 & 0 & 0 & 0 \\ 0 & 1 & 0 & 1 \\ 0 & 1 & 0 & 0 \end{bmatrix} \underline{y}_p(t) \end{aligned} \quad (95)$$

So with weightings on  $\epsilon$ ,  $\dot{\lambda}$ , and  $\dot{\epsilon}$  of 9, 4, and 1 respectively,  $Q_Y$  becomes

$$\begin{aligned} Q_Y &= (H')^T Q'_Y (H') \\ &= \begin{bmatrix} 9 & 0 & 0 & 0 \\ 0 & 5 & 0 & 4 \\ 0 & 0 & 0 & 0 \\ 0 & 4 & 0 & 4 \end{bmatrix} \end{aligned} \quad (96)$$

### The Pilot Model in Action

The objective of this chapter has been to present the equations and rationale of the Kleinman pilot model applied to the air-to-air tracking task. In practice the computations are performed by means of a digital computer program. As mentioned previously the program used in this study was adapted from that developed by Enright (Ref 2). A brief description of the program logic follows.

After the situational data, e.g., stability derivatives, velocities, altitudes, target noise covariance, etc., and cost functional weightings were input to the program, the feedback gains,  $\underline{g}$ , and consequently  $\tau_N$ , were computed. If the desired value of  $\tau_N$  was not achieved, the weighting on the control rate,  $g$ , was adjusted and the computations repeated. This process was repeated until the proper weighting had been discovered that yielded the desired  $\tau_N$ . The optimal feedback gains were now known.

The uncorrelated observation and motor noises were now added to the system in the form of initial guesses at the

values of their respective covariance matrices  $V_y$  and  $V_u$ . Enough information was now known to compute the error covariance,  $C$ , from equation (54). The covariances of the system states, which in the augmented form, included the control,  $u(t)$ , were then computed from equation (57). Finally new values for  $V_y$  and  $V_u$  were calculated using equations (69) and (70), respectively. If the differences between the new and old values of the noise covariances were not tolerable, the process was repeated until convergence to the correct covariances were achieved, within 5% tolerances. The RMS values of the pilot model performance parameters were then computed from equation (57) and (61).

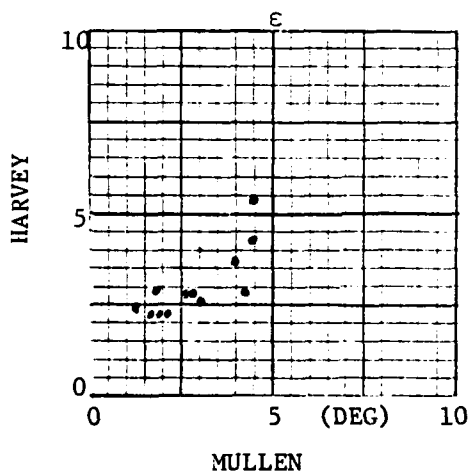
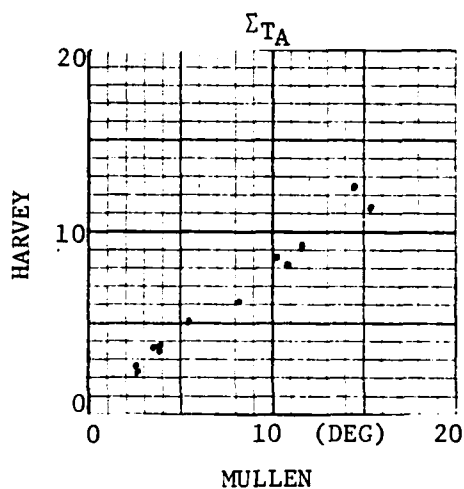
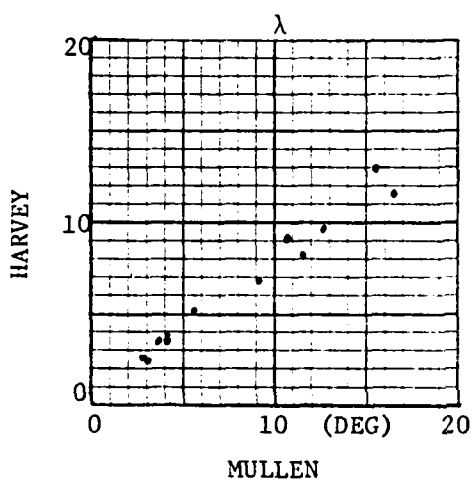
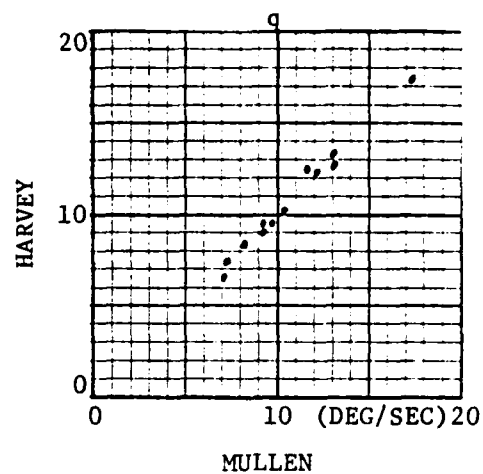
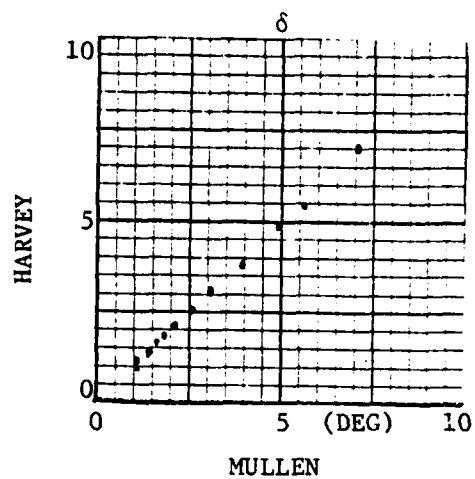
In the next section the actual results obtained from the analog simulation are compared for correlation with those obtained from the pilot model "flying" all twelve cases for each of the system modifications made to reflect the short term tracking task.



## V. Analysis of Results

The first task was to reproduce Harvey's final data using the OPM developed for this study. The results obtained from this model are compared with Harvey's in Fig 18 where each point is a plot of Harvey's RMS predicted value versus the value predicted by this study's OPM for the given case and performance variable. It can be seen that an almost one-to-one correlation exists for all variables except  $\epsilon$ . While discrepancies in  $\epsilon$  are apparent, it should be noted that Harvey's correlation for  $\epsilon$  with his experimental data was not as strong as that displayed by the other variables. The OPM used in this study was checked several times to assure no errors were present. Since none were found the next task was to determine how well the OPM would predict RMS performance for a short term tracking task. Figure 19 is a plot of the predicted RMS performance versus the actual short term tracking data collected using the hybrid simulation. The correlation is significantly poorer than that achieved in Ref 1 for a long term task. Consequently, effort was made to modify the OPM to produce better correlation. Several approaches were taken; their discussion follows.

The first approach was to change the system time constants, namely  $\tau_N$ , the neuromuscular delay constant and  $\tau$ , the perceptual delay constant. It was thought that compared to a pilot tracking a target for 100 seconds as in Ref 1, a



$$Q_y = \begin{bmatrix} 9 & 0 & 0 & 0 \\ 0 & 5 & 0 & 4 \\ 0 & 0 & 0 & 0 \\ 0 & 4 & 0 & 4 \end{bmatrix}$$

Figure 18. Comparison of RMS Performance Results Between Reference and This Study

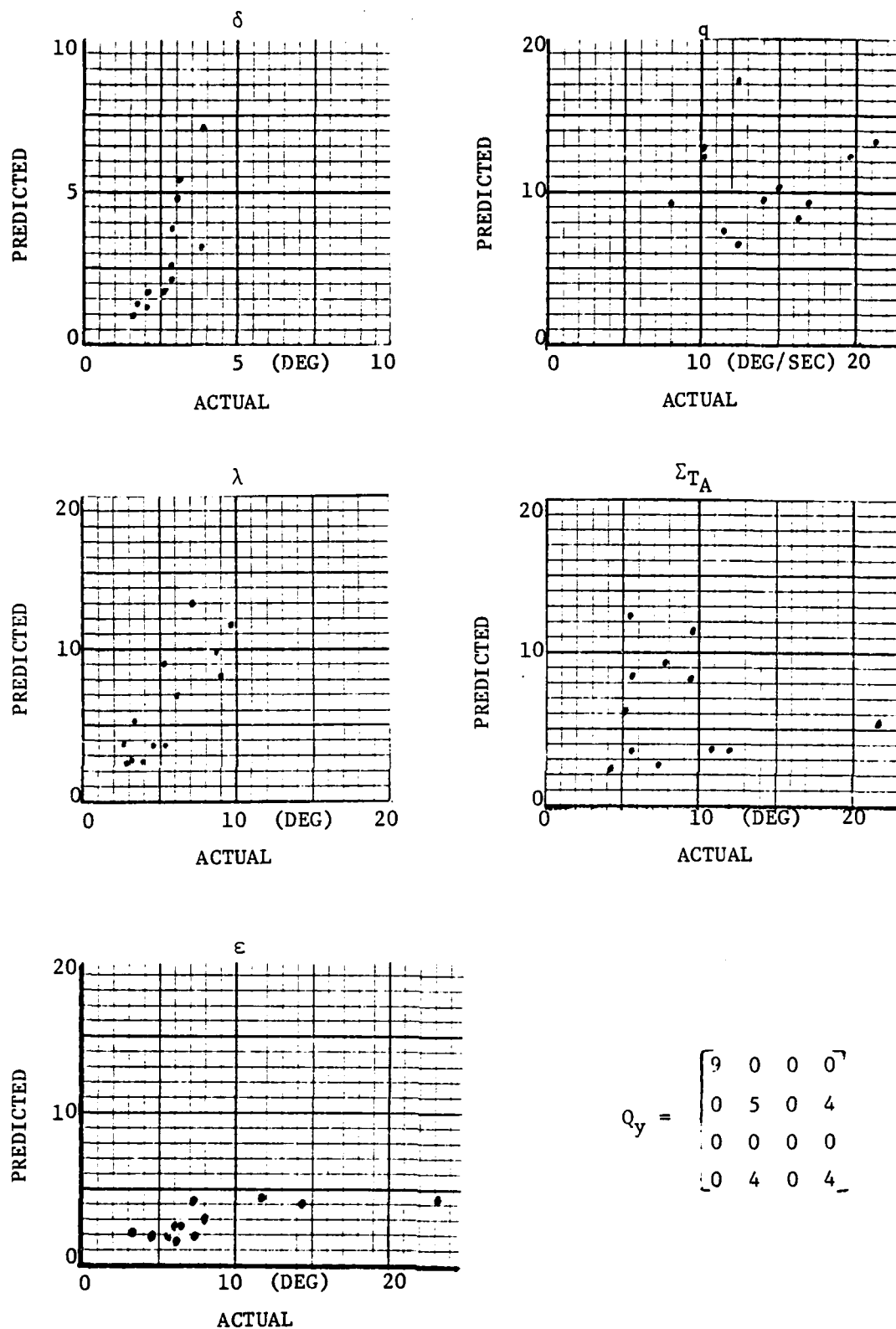
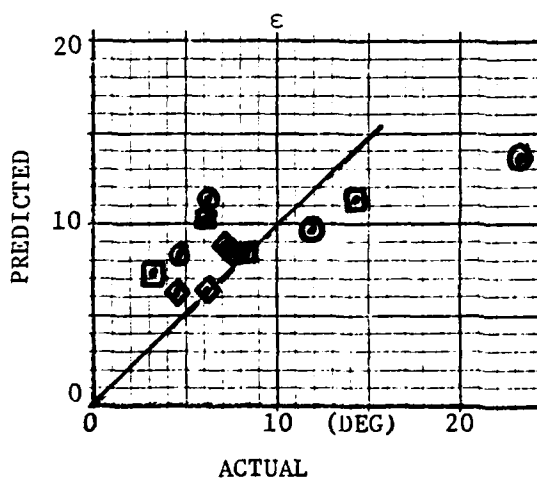
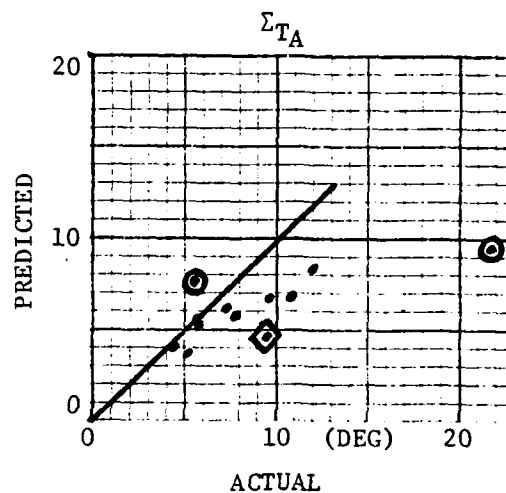
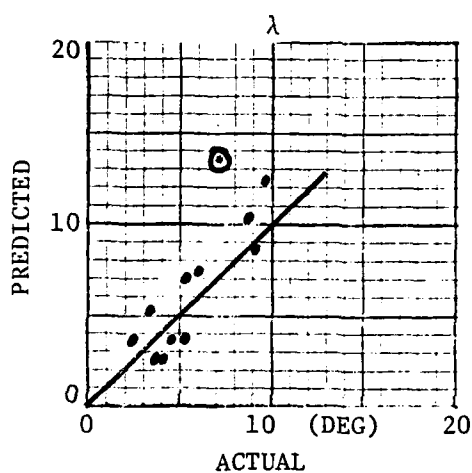
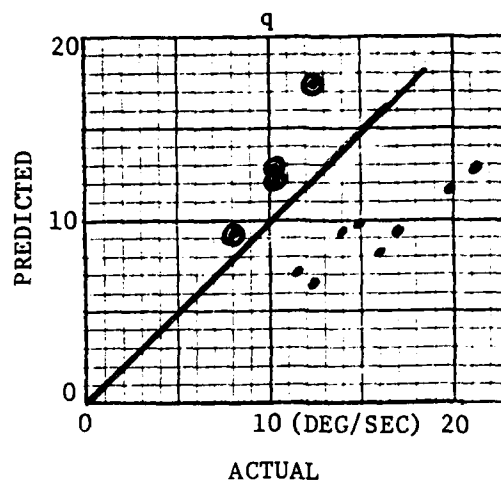
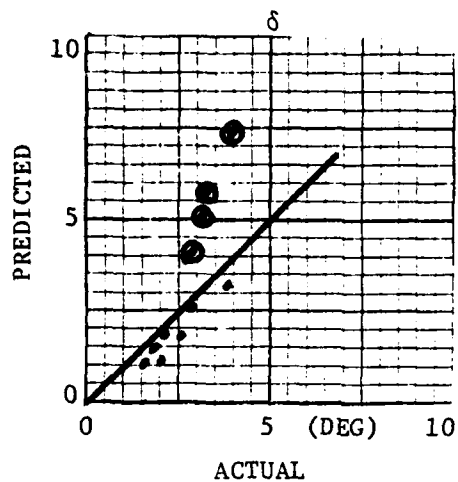


Figure 19. RMS Performance Comparison Between OPM Predicted vs Actual Hybrid Using  $Q_y$  Used for Long Term Tracking

pilot tracking a target for a short time, here 10 seconds, might be considered more alert and be capable of better concentration. This would effectively allow reductions in the values used for both  $\tau_N$  and  $\tau$ . The parameter  $\tau_N$ , was reduced from 0.1 to 0.07 seconds and  $\tau$  was reduced from 0.2 seconds to 0.15 seconds. Each change was examined separately; neither produced results that differed significantly from the previous results.

The next modification to the OPM was to vary  $Q_y$ , the observation weighting matrix. As a starting point Fig 19 was examined for possible clues as to which weighting matrix variables to change. One notes that a modest correlation for  $\delta$  and  $\lambda$  is evident while there is virtually no correlation for  $q$  or  $\Sigma_{TA}$ . Furthermore the tracking error,  $\epsilon$ , the most important variable in tracking tasks, shows a modest correlation between predicted and actual hybrid RMS results. Of note however is that with the  $\epsilon$  term of  $Q_y$  set at 9, the OPM overpenalizes predicted RMS excursions on  $\epsilon$  as the hybrid error is 3 to 4 times the predicted error in all cases. This observation suggests reducing the weighting term. The  $Q_{y\epsilon}$  term was decreased to 3, 0.1, and 0.05 and the OPM run for each case. The 0.1 weighting produces the best results. As shown in the graph in Fig 20 the correlation on  $\delta$ ,  $q$ , and  $\lambda$  is essentially unchanged, but both  $\Sigma_{TA}$  and  $\epsilon$  show improved correlation over the original  $Q_y$  weighting.

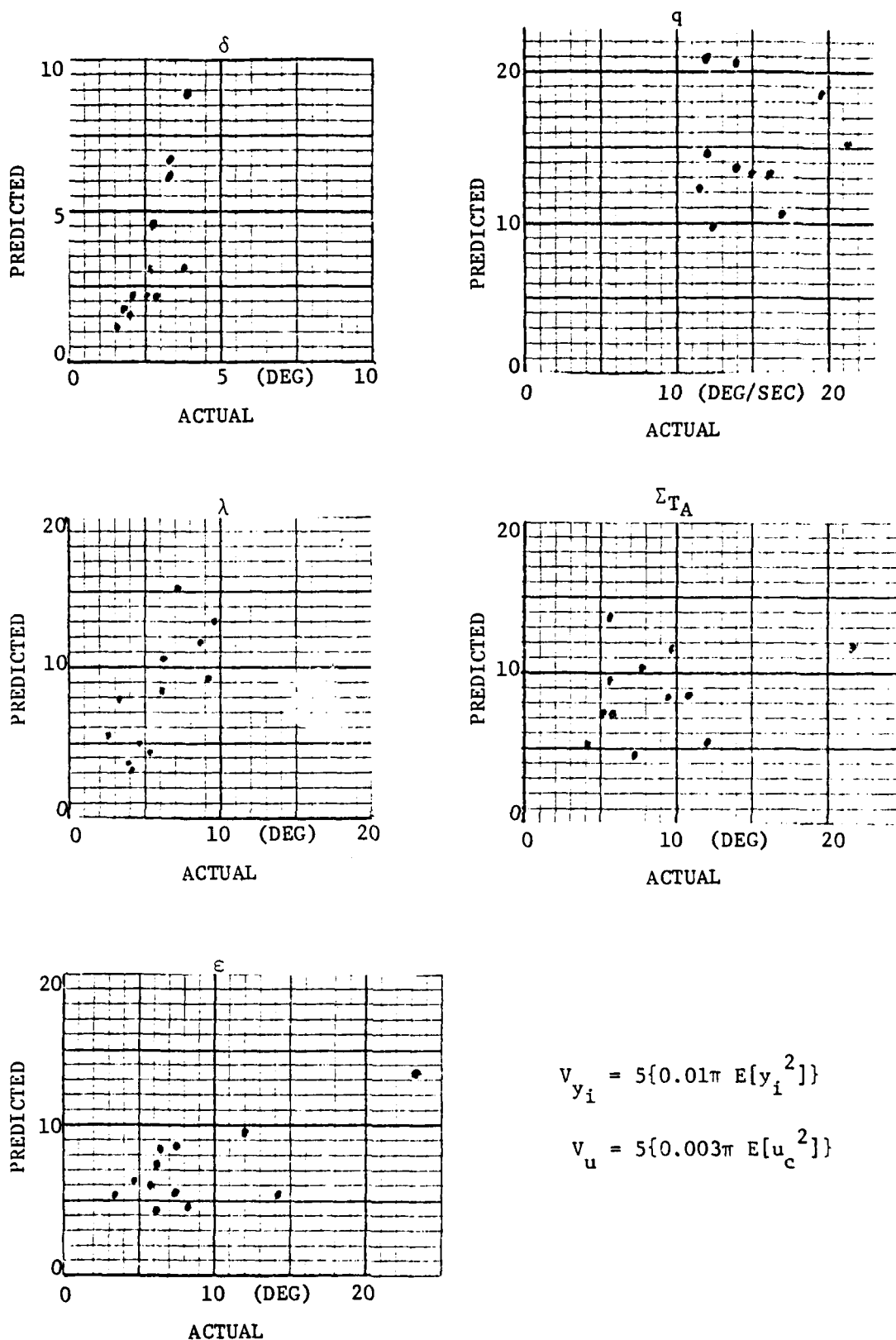
The next approach tried was to increase the observation



$$Q_y = \begin{bmatrix} .1 & 0 & 0 & 0 \\ 0 & 5 & 0 & 4 \\ 0 & 0 & 0 & 0 \\ 0 & 4 & 0 & 4 \end{bmatrix}$$

Legend: ○ A-7  
◇ F-5  
□ F-4E

Figure 20. RMS Comparison of Performance Results Using  $Q_y$  with Decreased Weighting on  $\epsilon$



$$V_{y_i} = 5\{0.01\pi E[y_i^2]\}$$

$$V_u = 5\{0.003\pi E[u_c^2]\}$$

Figure 21. RMS Performance Comparison from OPM  
Modelled with Increased Observer, Motor Noise

and motor noise strengths,  $V_{y_i}$  and  $V_u$ . These terms account for the random controller remnant modelled in the OPM. Increasing these quantities represents greater expected perturbations in pilot response characteristics and in the random errors encountered while observing the displayed variables (Ref 2:359). Such additional "confusion" on the part of the pilot might be considered to result from insufficient training prior to performing the actual runs from which the data was taken; i.e. on occasion the opposite  $\delta_c$  might have been applied to track the target as required. To produce this change, the strength of the motor and observation noises,  $V_{y_i}$  and  $V_u$ , were increased by a factor of 5 by scaling equations (69) and (70) accordingly. The correlation thus obtained is shown in the graphs of Fig 21. There is a slight improvement on  $\epsilon$  but correlation on the other parameters was essentially unchanged from the original  $Q_y$  weighting results.

During the actual hybrid runs it was noted that each pilot had great difficulty in tracking the target when "flying" the A-7 in that for short times the target would actually disappear from the screen. Examination of Fig 20 shows that almost all A-7 cases are plotted away from the main trend line formed by the F-4E and F-5 cases. For  $\delta$  and  $q$  the A-7 cases appear to form their own trend while for  $\lambda$ ,  $\Sigma_{T_A}$ , and  $\epsilon$ , the demarcation is not so distinct. In order to find a  $Q_y$  weighting matrix that might model what seems to be "bad" data

points, it was considered that the pilot in these cases, was primarily concerned with  $\Sigma_{TA}$ , the relative line of sight between the target and attacker. Thus for these few cases his main concern was to keep the target on the screen. To reflect this approach, equal weightings of 1 were set on each of  $\Sigma_{TA}$  and  $\dot{\Sigma}_{TA}$  with zero weightings on  $\epsilon$  and  $\dot{\epsilon}$ . Unfortunately the predicted results were less correlated than even for the original case.

The final  $Q_y$  weighting considered was that of equal weightings of 1 on each of  $\epsilon$  and  $\dot{\epsilon}$  and zero weighting on  $\Sigma_{TA}$  and  $\dot{\Sigma}_{TA}$ . The results from this run, which incidently was the first  $Q_y$  weighting considered by Harvey, produced less correlation than that observed in the original case.

Since changing neither the time constants nor the  $Q_y$  weighting matrix seemed to provide satisfactory correlation between predicted and actual performance, a change was made in the method of calculating the predicted values. These values are calculated from the covariance matrix of the augmented state vector  $\underline{z}(t)$  via solution to equation (57), and more specifically from the third term which is the dominant steady-state component of the covariance matrix. Computation of this term was performed via the subroutine MLINEQ (Ref 4) which solves Lyapunov equations of the form of (60) using linear matrix equation techniques. It presupposed a steady state solution in that it required by definition integration



of the third term over the infinite interval  $[0, \infty]$ . Since the integration interval here was over  $[0, 10]$ , it was thought that a subroutine that would actually perform the integration over this finite interval might produce better correlation. The subroutine INTEG, one of the Kleinman subroutines (Ref 4), was inserted to replace MLINEQ and the sample cases were run using the original  $Q_y$  weighting. The results thus predicted indicate RMS values of  $\delta$ ,  $q$ , and  $\lambda$  much less than that recorded in the actual hybrid simulation; overall correlation was poor. These results, along with those of previous cases, are tabulated in Appendix C.

## VI. Conclusions and Recommendations

### Conclusions

The OPM used in this study to model the short term tracking task was moderately successful in obtaining correlation between the OPM predicted performance parameters and those obtained from actual hybrid simulation with a pilot-in-the-loop. The correlation was not as good as that obtained for the long term task (Ref 1) but definite trends were evident.

The conclusions reached on the four methods used to attempt to modify the OPM to reflect the short term tracking task are as follows.

a) Decreasing  $\tau_N$ ,  $\tau$ .

The OPM is effectively unchanged in its predictions as a result of decreasing  $\tau_N$  by 30% and  $\tau$  by 25%.

b) Increasing  $V_{y1}$  and  $v_u$  by Factor of 5.

This approach is considered ineffective. While modestly improving the correlation for  $\epsilon$ , the correlation for  $q$  was degraded. No significant improvement was made overall.

c) Changing Integration Time Interval for Covariance Calculation.

This approach is judged most ineffective as it implied that much less elevator is required to track the target than that which was actually

recorded by the man-in-the-loop hybrid simulation.

d) Changing  $Q_y$  Weighting Matrix.

This approach is judged the most effective of the four methods used. By decreasing the weighting on the  $Q_y(\epsilon)$  term, the best correlation of all efforts was attained (Fig 20) with reasonably good correlation for  $\delta$ ,  $q$ , and  $\lambda$  and an evident trend to  $\Sigma_{TA}$  and  $\epsilon$ .

One notes however two different correlation lines for  $\delta$  and  $q$  and the seemingly misplaced data points for  $\lambda$ ,  $\Sigma_{TA}$ , and  $\epsilon$ . As stated earlier these points correspond to the A-7 aircraft dynamics. It is felt that their displacement results from the commanded elevator deflection to stick force gradient ( $K_F$ ) which was made the same for all three attacker aircraft. It is possibly too low for the A-7 in the flight regime modelled (15,000 ft,  $M=0.6$ ). Both the F-4E and F-5 were able to generate RMS performance statistics that correlated reasonably well with that predicted by the OPM with  $K_F = 0.005$  rad/lb<sub>F</sub>, but the A-7 at this  $K_F$  appears to have been unable to command sufficient  $\delta$  and hence  $q$  and  $\lambda$  to keep the correlation points of these variables in line with those of the F-4E and F-5. In hindsight it is felt an increased value of  $K_F$  for the A-7 might have brought the A-7 points in line with the F-4E and F-5.

### Recommendations

The following ideas are recommended for possible further study in order to improve the correlation between predicted and actual performance statistics:

- a) a more exhaustive investigation of changes to the  $Q_y$  weighting matrix for the cases studied here;
- b) more runs by each pilot for each case to establish a higher confidence level of hybrid data results (i.e. 10 or more runs versus the 5 runs/case/pilot made here);
- c) use of a different force stick that would allow sufficient stick travel to trim the aircraft so that the pilot would not be required to engage negative "G" maneuvers to track the target. The pilots commented that if at all possible negative "G" maneuvers are avoided in flight; and
- d) an investigation of the effect of different sampling rates of the output by the hybrid computer. The recorded variables were sampled at 100 Hz in this study, providing 1000 data points from which the variance was calculated digitally. It was suggested that some of the dispersion in the results might possibly have been due to a sampling rate that was too low.

## Bibliography

1. Harvey, Thomas R. Application of an Optimal Control Pilot Model to Air-to-Air Combat. AFIT Thesis GA/MA/74M-1. Wright Patterson Air Force Base, Ohio: Air Force Institute of Technology, March, 1974.
2. Kleiman, D. L., S. Baron and W. H. Levison. "An Optimal Control Model of Human Response, Part 1", Automatica, 6: 357-363 (May 1970).
3. Roskam, Jan. Airplane Flight Dynamics and Automatic Flight Controls, Roskam Aviation and Engineering Corporation; Lawrence, Kansas; 1979.
4. Kleinman, David L. "Computer Programs Useful in Linear System Studies", SCI Technical Memorandum, Systems Control Inc., Palo Alto, California, 1971.
5. Enright, Randall. Predicting Pilot Opinion Rating of Flying Qualities of Highly Control-Augmented Aircraft Using Optimal Pilot Model. AFIT Thesis GAE/AA/80D-3. Wright Patterson Air Force Base, Ohio: Air Force Institute of Technology, December 1980.
6. McRuer, D., Askenas, I., Graham, D., Aircraft Dynamics and Automatic Control, Princeton University Press, Princeton, New Jersey; 1973.
7. Baron, S., et al. Application of Optimal Control Theory to the Prediction of Human Performance in a Complex Task. AFFDL-TR-69-81. Wright Patterson Air Force Base, Ohio: Air Force Institute of Technology, December, 1973.
8. Abramowitz, M. and Stagun, I. Handbook of Mathematical Functions and Formulas, Graphs and Mathematical Tables, U.S. Dept. of Commerce, National Bureau of Standards.
9. Maybeck, Peter S. Stochastic Models, Estimation and Control, Vol. 1, Academic Press, 111 Fifth Ave., New York, New York; 1979.
10. Graham, Dunstan and McRuer. Analysis of Non-Linear Control Systems; Dover Publications, New York; 1971.
11. Kleinman, David L. and Sheldon Baron. Analytic Evaluation of Display Requirements for Approach to Landing, NASA CR-1952; 1971.

12. Bryan, Ralph S. Unpublished report on ballistics modelling. AFWAL/AART, Wright Patterson Air Force Base, Ohio: Air Force Avionics Laboratory, July 1973.
13. Schmidt, David K. "Pilot-Optimal Augmentation for the Air-to-Air Tracking Task", Journal of Guidance and Control, Sept-Oct 1980.

## Appendix A

### Determination of Projectile Time of Flight and Average Relative Velocity

Equation (16), used to compute the required lead angle  $\lambda$  is dependent on three projectile trajectory parameters whose values require a priori calculation:

$T_f$  = time of flight of projectile to impact point

$V_f$  = average relative velocity of projectile over this time of flight

$k$  = drag scaling factor

For simplicity it was assumed that the weapon was colinear with the attacker's velocity vector.

#### Time of Flight, $T_f$

To obtain  $T_f$ , equate expressions for the range at intercept of the bullet and target and then solve the resulting equation for  $T_f$ . For this calculation it is assumed the target is in a constant normal acceleration maneuver as depicted in Figure A-1.

The expression for target range from the point of fire is

$$R_T = \sqrt{R_{T_x}^2 + R_{T_y}^2} \quad (A-1)$$

From Fig. A-1

$$\begin{aligned} R_{T_x} &= D + \int_0^{T_f} V_{T_x} dt \\ &= D + \frac{V_T}{\gamma_T} \sin \gamma_T T_f \end{aligned} \quad (A-2)$$

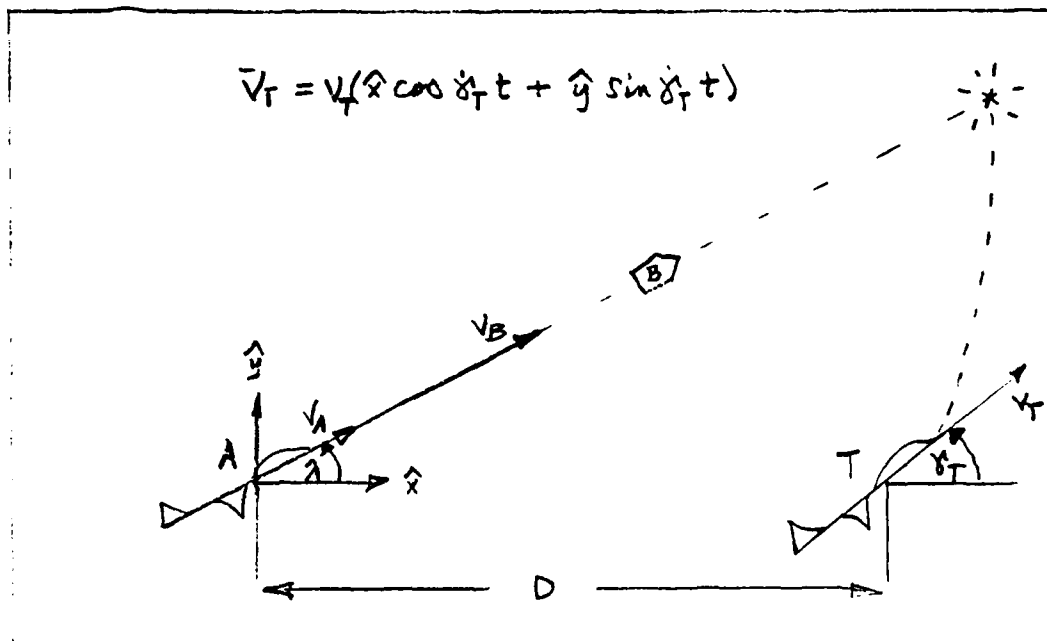


Figure A-1. Projectile Trajectory Geometry

and

$$R_{T_Y} = \int_0^{T_f} V_{T_Y} dt = \frac{V_T}{\dot{\delta}_T} (1 - \cos \dot{\delta}_T T_f) \quad (A-3)$$

where  $V_T$  is the target velocity and  $\dot{\delta}_T$  is the target angular velocity given by

$$\dot{\delta}_T = -\frac{1}{V_T} A_{Z_T} \quad (A-4)$$

The expression for bullet range is obtained from application of Newton's II law to the bullet giving

$$M_B \dot{V}_{B/O} = F_{\text{Drag}} = -\frac{1}{2} \rho V_{B/O}^2 A_B C_{D_B} \quad (A-5)$$



where  $A_B$  is the bullets cross sectional area and  $C_{D_B}$  is the aerodynamic drag coefficient whose dependence on Mach number is approximated by

$$C_{D_B} \simeq b/\sqrt{v_{B/O}} \quad (A-6)$$

This form is commonly used and gives good results (Ref 12) since the bullet is always supersonic for the time of flight range considered in this study. It is also assumed that for time of flight calculation any gravity drop during flight is offset by the resistance met due to increasing air density. Hence (A-5) becomes

$$\dot{v}_{B/O} = -\left(\frac{1}{2} \frac{A_B}{m_B} \rho b\right) v_{B/O}^{3/2} \quad (A-7)$$

or in terms of current ballistic modelling (Ref 12:3)

$$\dot{v}_{B/O} = -2K_B (\rho/\rho_o) v_{B/O}^{3/2} \quad (A-8)$$

where  $K_B$  is the ballistic constant encompassing the bullet mass  $m_B$ , bullet cross sectional area  $A_B$  and drag curve constant  $b$ . The value of  $K_B = 0.00614$  was used in this study, the same as used by Harvey (Ref 1). The variables  $\rho$  and  $\rho_o$  represent the air density at altitude and sea-level respectively. Integrating (A-8) gives

$$\int_{v_{B_i}}^{v_B(t)} \frac{dv_{B/O}}{v_{B/O}^{3/2}} = - \int_0^t 2K_B (\rho/\rho_o) dt \quad (A-9)$$

where  $V_{B_i}$  is the initial bullet velocity given by

$$V_{B_i} = V_{B/A} + V_{A/O} \quad (A-10)$$

Equation (A-9) gives

$$V_B(t) = \left[ K_B (\rho/\rho_o) t + 1/\sqrt{V_{B_i}} \right]^{-2} \quad (A-11)$$

The range of the bullet from the point of fire is then

$$\begin{aligned} R_B(T_f) &= \int_0^{T_f} V_B(t) dt \\ &= \frac{V_{B_i} T_f}{1 + K_B (\rho/\rho_o) \sqrt{V_{B_i}} T_f} \end{aligned} \quad (A-12)$$

Determination of  $T_f$  was performed via a Newton-Raphson root-solving routine to solve

$$R_B(T_f) = R_T(T_f) \quad (A-13)$$

for each of the 12 cases studied.

#### Average Relative Bullet Velocity, $V_f$

The average bullet velocity along the flight trajectory is obtained from

$$V_{avg} = \frac{1}{T_f} \int_0^{T_f} V_B(t) dt \quad (A-14)$$

$$\begin{aligned} \text{SO} \quad V_{avg} &= \frac{1}{T_f} R_B(T_f) = \frac{V_{B_i}}{1 + K_B (\rho/\rho_o) \sqrt{V_{B_i}} T_f} \\ &= k V_{B_i} \end{aligned} \quad (A-15)$$

where  $k$  is a scaling parameter that reduces the initial bullet velocity  $V_{B_i}$ , to an effective average velocity over the flight trajectory due to the viscous drag encountered. Hence the average relative velocity of the bullet, with respect to the attacker, is

$$V_f = V_{avg} - V_{A/O} \quad (A-16)$$

## Appendix B

### Algorithm Used To Generate White Noise Source

FUNCTION RNG (SV, SD)

INTEGER SV

---

FIND A PSEUDO-RANDOM NUMBER FROM AN LATECHY PSEUDO-RANDOM NUMBER GENERATOR

RANGE : -1 TO 1

SV IS THE SEED FOR THE NEXT RANDOM NUMBER FROM RNG.  
THE FIRST VALUE OF SV MUST BE SUPPLIED BY THE CALLING  
PROGRAM. NOTE IT CAN NOT BE A LITERAL.

---

Z = ABS(RNG(SV))

R = ABS(RNG(SV))

---

RATIONAL APPROXIMATION TO VALUE, Y, WHICH DEFINES  
THE LOWER END OF THE RIGHT SIDE OF A NORMAL DISTRIBUTION  
WITH AREA OF 2(>=) AND (<=).

---

FROM "HANDBOOK OF MATHEMATICAL FUNCTIONS WITH FORMULAS,  
GRAPHS, AND MATHEMATICAL TABLES", EDITED  
BY MILTON ABRAMOWITZ AND IRVING A. STEGUN  
EQUATION 26.2.23\* PAGE 572

---

IF (7.61..5) Z = 1.-Z

E = EXP(ALOG(1./Z\*\*2))

Y1 = 2.515517 + E\*(.802853 + E\*.010328)

X1 = 1. + E\*(1.432788 + E\*(.189269 + E\*.001308))

Y2 = 1.-X1/Y1

---

IF (8.11..5) X2 = -X1

THIS GENERATES A NORMAL DISTRIBUTION OF RANDOM NUMBERS  
WITH A MEAN OF APPROXIMATELY ZERO AND A STANDARD DEVIATION  
OF 1.

---

THE STANDARD DEVIATION CAN BE CHANGED BY USING THE FOLLOWING:

RND = X2\*SD

WHERE SD IS THE STANDARD DEVIATION

RETURN

RND

26.2.25

$$r_p = t - \frac{c_0 + c_1 t + c_2 t^2}{1 + d_1 t + d_2 t^2 + d_3 t^3} + \epsilon(p), \quad t = \sqrt{\ln \frac{1}{p}}$$

$$|\epsilon(p)| < 4.5 \times 10^{-4}$$

$$c_0 = 2.515517 \quad d_1 = 1.432788$$

$$c_1 = .802853 \quad d_2 = .189269$$

$$c_2 = .010328 \quad d_3 = .001308$$

Appendix C

Tabulation of Hybrid Simulation Results and of  
OPM Predicted vs Actual Hybrid Results

# Tabulation of Hybrid Simulation Data

- RMS Results from the Three Pilots
- Tracking Time = 10 seconds

CASE	Elevator ( $\delta$ ) (Degrees)			Pitch Rate ( $\dot{q}$ ) (Deg/sec)			Lead Angle ( $\lambda$ ) (Degrees)			LOS ( $\hat{\lambda}_A$ ) (Degrees)			Error ( $\epsilon$ ) (Degrees)		
	1	2	3	1	2	3	1	2	3	1	2	3	1	2	3
Range/ $A_z \eta$															
F4E-1000/3.5	2.49	3.01	3.38	18.6	15.3	17.2	4.15	3.78	4.32	5.29	10.2	6.01	4.88	11.5	8.47
-1000/5.0	2.88	4.09	4.26	20.2	21.9	21.7	4.68	5.57	5.58	8.41	14.4	13.2	9.51	16.7	16.9
-3000/3.5	1.63	2.51	2.43	10.3	13.0	11.3	4.03	7.55	6.78	3.20	6.61	5.40	3.56	4.12	2.70
-3000/5.0	1.87	3.18	3.10	11.6	18.0	15.4	6.12	10.7	9.68	4.95	11.2	7.13	4.15	7.72	6.50
F5 -1000/3.5	1.34	2.39	2.34	11.2	18.4	18.7	2.72	4.53	4.33	2.84	5.80	4.60	2.76	5.72	5.90
-1000/5.0	1.82	2.92	2.98	15.5	21.5	22.1	3.59	5.39	5.23	6.92	5.65	4.61	8.50	7.52	6.35
-3000/3.5	1.43	1.74	1.71	11.3	13.3	12.5	7.63	9.83	9.78	12.0	8.44	8.12	10.1	4.16	4.10
-3000/5.0	1.57	2.05	1.84	12.9	15.4	13.7	8.35	11.1	9.58	9.52	11.4	8.03	7.70	11.0	3.73
A7 -1000/3.5	3.16	3.24	3.50	10.1	9.58	10.9	2.58	2.52	2.77	7.76	11.8	13.2	8.65	12.6	14.6
-1000/5.0	3.86	4.31	3.78	12.6	14.5	10.5	3.38	3.80	2.75	10.3	24.1	31.4	12.3	24.9	32.9
-3000/3.5	2.74	2.97	3.16	8.18	8.04	7.98	5.71	6.46	6.71	4.30	7.28	5.60	2.72	7.35	7.44
-3000/5.0	2.94	3.57	3.55	9.83	11.0	10.5	6.10	7.79	7.35	4.76	6.91	4.78	5.12	6.22	7.33

Tabulation of Predicted vs Actual Results

•original case with  $Q_y =$

$\begin{bmatrix} 9 & 0 & 0 & 0 \\ 0 & 5 & 0 & 4 \\ 0 & 0 & 0 & 0 \\ 0 & 4 & 0 & 4 \end{bmatrix}$

CASE	Elevator( $\delta$ ) (Degrees)		Pitch Rate( $\dot{\phi}$ ) (Deg/sec)		Lead Angle( $\lambda$ ) (Degrees)		LOS( $\Sigma_A$ ) (Degrees)		Error( $\epsilon$ ) (Degrees)	
	Act	Pred	Act	Pred	Act	Pred	Act	Pred	Act	Pred
Range/ $A_{zT}$										
F4E-1000/3.5	2.96	2.15	17.0	9.48	4.08	2.72	7.17	2.72	8.28	3.01
-1000/5.0	3.74	3.04	21.3	13.3	5.34	3.82	12.0	3.75	14.3	4.04
-3000/3.5	2.19	1.79	11.5	7.42	6.12	6.98	5.07	6.09	3.46	2.07
-3000/5.0	2.72	2.54	15.0	10.2	8.83	9.96	7.76	9.13	6.12	2.75
F5 -1000/3.5	2.02	1.20	16.1	8.22	3.86	2.49	4.41	2.33	4.79	2.01
-1000/5.0	2.57	1.74	19.7	12.3	4.74	3.63	5.72	3.60	7.47	4.25
-3000/3.5	1.63	1.00	12.4	6.73	9.08	8.24	9.52	8.04	6.13	1.34
-3000/5.0	1.82	1.42	14.0	9.59	9.68	11.7	9.65	11.4	7.48	1.89
A7 -1000/3.5	3.30	4.93	10.2	12.4	2.62	3.61	10.9	3.63	11.9	4.41
-1000/5.0	3.98	7.01	12.5	17.3	3.31	5.12	21.9	5.07	23.4	4.49
-3000/3.5	2.96	3.83	8.07	9.05	6.29	9.02	5.71	8.58	5.84	1.77
-3000/5.0	3.35	5.49	10.4	12.8	7.08	13.0	5.48	12.4	6.21	2.69

# Tabulation of Predicted vs Actual Results

• weighting on  $\epsilon$  term of  $Q_y$  decreased to 0.1 to give  $C_y = \begin{bmatrix} 0.1 & 0 & 0 & 0 \\ 0 & 5 & 0 & 4 \\ 0 & 0 & 0 & 0 \\ 0 & 4 & 0 & 4 \end{bmatrix}$

CASE	Elevator( $\delta$ ) (Degrees)		Pitch Rate( $\dot{q}$ ) (Deg/sec)		Lead Angle( $\lambda$ ) (Degrees)		LOS( $\Sigma \alpha$ ) (Degrees)		Error( $\epsilon$ ) (Degrees)	
	Act	Pred	Act	Pred	Act	Pred	Act	Pred	Act	Pred
F4E-1000/3.5	2.96	2.26	17.0	9.09	4.08	2.73	7.17	6.13	8.28	8.35
	3.74	3.20	21.3	12.8	5.34	3.86	12.0	8.30	14.3	11.4
	2.19	1.88	11.5	7.07	6.12	7.37	5.08	3.87	3.46	7.46
	2.72	2.66	15.0	9.96	8.83	10.4	7.76	5.59	6.12	10.0
F5 -1000/3.5	2.02	1.25	16.1	8.19	3.86	2.56	4.41	4.04	4.79	6.16
	2.57	1.77	19.7	11.6	4.74	3.63	5.72	5.50	7.47	8.47
	1.63	1.05	12.4	6.71	9.08	8.77	9.52	4.68	6.13	6.11
	1.82	1.47	14.0	9.43	9.68	12.4	9.65	6.96	7.48	7.88
A7 -1000/3.5	3.30	5.22	10.2	12.3	2.62	3.75	10.9	6.69	12.0	9.64
	3.98	7.42	12.5	17.4	3.31	5.33	21.9	9.31	23.4	13.5
	2.96	4.07	8.07	9.13	6.29	6.96	5.71	5.45	5.84	8.29
	3.35	5.76	10.4	12.8	7.08	13.6	5.48	7.86	6.21	11.1



# Tabulation of Predicted vs Actual Results

- observation noise and motor noise strength increased by factor of 5

CASE	Elevator( $\delta$ ) (Degrees)		Pitch Rate( $\dot{\varphi}$ ) (Deg/sec)		Lead Angle( $\lambda$ ) (Degrees)		LOS( $\Sigma\lambda$ ) (Degrees)		Error( $\epsilon$ ) (Degrees)	
	Act	Pred	Act	Pred	Act	Pred	Act	Pred	Act	Pred
F4E-1000/3.5 -1000/5.0 -3000/3.5 -3000/5.0	2.96	2.28	17.0	10.8	4.08	3.09	7.17	3.83	8.28	4.71
	3.74	3.22	21.3	15.2	5.34	4.33	12.0	5.23	14.3	6.41
	2.19	2.22	11.5	12.1	6.12	8.34	5.07	7.25	3.46	5.35
	2.72	3.15	15.0	17.1	8.83	11.8	7.76	10.3	6.12	7.35
F5 -1000/3.5 -1000/5.0 -3000/3.5 -3000/5.0	2.02	1.58	16.1	13.2	3.86	3.57	4.41	5.18	4.79	6.25
	2.57	2.23	19.7	18.6	4.74	5.04	5.72	7.23	7.47	8.72
	1.63	1.27	12.4	9.79	9.08	9.19	9.52	8.25	6.13	4.27
	1.82	1.87	12.0	13.7	9.68	13.0	9.65	11.7	7.48	5.62
A7 -1000/3.5 -1000/5.0 -3000/3.5 -3000/5.0	3.30	6.26	10.2	21.0	2.62	5.57	10.9	8.25	6.13	4.27
	3.98	8.91	12.5	30.0	3.31	7.72	21.9	11.9	23.4	13.5
	2.96	4.72	8.07	14.4	6.29	10.6	5.71	9.57	5.84	5.98
	3.35	6.72	10.4	20.5	7.08	15.1	5.48	13.6	6.21	8.36

AD-A115 543

AIR FORCE INST OF TECH WRIGHT-PATTERSON AFB OH SCHOOL--ETC F/6 17/8  
PREDICTION OF SHORT TERM TRACKING TASKS USING AN OPTIMAL PILOT --ETC(U)  
MAR 82 P A MULLEN  
AFIT/OAE/AA/81D-21

UNCLASSIFIED

NL

219 2  
D-5543



					END DATE FILMED 7-82 DTIC
--	--	--	--	--	---------------------------------------

# Tabulation of Predicted vs Actual Results

• steady state results calculated using  
 INTEG VS MLINEQ with original  $Q_y$  of  $Q_y = \begin{bmatrix} 9 & 0 & 0 & 0 \\ 0 & 5 & 0 & 4 \\ 0 & 0 & 0 & 0 \\ 0 & 4 & 0 & 4 \end{bmatrix}$

CASE	Elevator( $\delta$ ) (Degrees)		Pitch Rate( $\dot{q}$ ) (Deg/sec)		Lead Angle( $\lambda$ ) (Degrees)		LOS( $\Sigma_A$ ) (Degrees)		Error( $\epsilon$ ) (Degrees)	
	Act	Pred	Act	Pred	Act	Pred	Act	Pred	Act	Pred
F4E-1000/3.5	2.96	0.49	17.0	1.03	4.08	0.34	7.17	10.0	8.28	9.81
	3.74	0.68	21.3	1.41	5.34	0.46	12.0	13.8	14.3	13.5
	2.19	0.84	11.5	0.21	6.12	0.36	5.07	2.96	3.46	2.90
	2.72	0.16	15.0	0.30	8.83	0.42	7.76	2.55	6.12	3.26
F5	2.02	0.47	16.1	1.02	3.86	0.30	4.41	7.10	4.79	6.95
	2.57	0.65	19.7	1.37	4.74	0.40	5.72	9.68	7.47	9.48
	1.63	0.10	12.4	0.21	9.08	0.31	9.52	2.30	6.13	2.12
	1.82	0.12	14.0	0.26	9.68	0.39	9.65	2.88	7.48	2.65
A7	3.30	0.19	10.2	0.34	2.62	0.21	10.9	8.31	12.0	8.17
	3.98	0.26	12.5	0.46	3.31	0.29	21.9	11.4	23.4	11.2
	2.96	0.04	8.07	0.06	6.29	0.16	5.71	2.80	5.84	2.69
	3.35	0.05	10.4	0.09	7.08	0.21	5.48	3.52	6.21	3.30

Appendix D

Summary of Pilot Flying Experience

Pilot	Type Aircraft	Hours Flown This Aircraft
Pilot #1	F-4	1200
	F-15	700
Pilot #2	F-4	1000
	F-105	800
Pilot #3	F-4	2000
	F-15	1000

## VITA

Patrick A. Mullen was born in 1951 at Walkerton, Ontario, Canada. He completed his high school education there and proceeded to the University of Waterloo, Waterloo, Ontario to study Physics. In 1971 he joined the Canadian Armed Forces via the Regular Officer Training Program. In 1974 he graduated with a Bachelor of Science degree in Physics and was subsequently commissioned as a First Lieutenant in the CF.

His first assignment was as a maintenance officer on a VIP transport squadron. This was followed in 1977 by a tour at NDHQ, Ottawa as a program manager on new aircraft related capital acquisition programs. In 1980 he was selected to attend AFIT to study Air Weapons engineering. He graduated with a Master of Science degree in Aeronautical Engineering, specializing in Guidance and Control and Air Weapons in March, 1982.

Permanent address: 214 Princess Street  
Walkerton, Ontario  
Canada

UNCLASSIFIED

SECURITY CLASSIFICATION OF THIS PAGE (When Data Entered)

REPORT DOCUMENTATION PAGE		READ INSTRUCTIONS BEFORE COMPLETING FORM
1. REPORT NUMBER GAE/AA/81D-21	2. GOVT ACCESSION NO. AD-A115543	3. RECIPIENT'S CATALOG NUMBER
4. TITLE (and Subtitle) PREDICTION OF SHORT TERM TRACKING TASKS USING AN OPTIMAL PILOT MODEL		5. TYPE OF REPORT & PERIOD COVERED MS Thesis
7. AUTHOR(s) Patrick A. Mullen Captain, Canadian Armed Forces		6. PERFORMING ORG. REPORT NUMBER
9. PERFORMING ORGANIZATION NAME AND ADDRESS Air Force Institute of Technology (AFIT-EN) Wright-Patterson AFB, Ohio 45433		8. CONTRACT OR GRANT NUMBER(s)
11. CONTROLLING OFFICE NAME AND ADDRESS		10. PROGRAM ELEMENT, PROJECT, TASK AREA & WORK UNIT NUMBERS
12. REPORT DATE March, 1982		13. NUMBER OF PAGES 83
14. MONITORING AGENCY NAME & ADDRESS (if different from Controlling Office)		15. SECURITY CLASS. (of this report) Unclassified
16. DISTRIBUTION STATEMENT (of this Report)  Approved for public release; distribution unlimited		15a. DECLASSIFICATION/DOWNGRADING SCHEDULE
17. DISTRIBUTION STATEMENT (of the abstract entered in Block 20, if different from Report)  15 APR 1982		
18. SUPPLEMENTARY NOTES  Approved for public release; IAW AFR 190-17 FREDRICK C. LYNCH, Major, USAF Dean for Research and Director of Public Affairs Professional Development Air Force Institute of Technology (ATC) Wright-Patterson AFB, OH 45433		
19. KEY WORDS (Continue on reverse side if necessary and identify by block number) Air-to-Air Combat Optimal Control Pilot Modelling Analog/Hybrid Computer Simulation Kalman Filter Application		
20. ABSTRACT (Continue on reverse side if necessary and identify by block number) An optimal pilot model has previously been successful in pre- dicting the long term tracking performance of a longitudinal air- to-air gunnery task. This study investigated modifications to the same pilot model to determine whether it could be used to success- fully predict performance for a short term task. The same task, including a lead computing optical sight, was simulated on a hybrid computer. Three pilots flew three different aircraft configurations		

DD FORM 1 JAN 73 1473

EDITION OF 1 NOV 68 IS OBSOLETE

UNCLASSIFIED

SECURITY CLASSIFICATION OF THIS PAGE (When Data Entered)

UNCLASSIFIED

SECURITY CLASSIFICATION OF THIS PAGE(When Data Entered)

## 20. ABSTRACT

on the fixed-base simulator against a target driven to RMS accelerations of 3.5G and 5.0G by filtered, Gaussian noise. The target was at either 1000' or 3000' range. Averaged RMS data were recorded on the attacker's elevator deflection, pitch rate, lead angle, line of sight angle, and tracking error for each case. The identical task was modelled and analyzed using a digital pilot model formulated from optimal control theory. Modifications to this pilot model were made to reflect the short term tracking assignment. A comparison of the data generated by the human pilots versus that of the optimal pilot model showed moderate correlation for elevator deflection, lead angle, and pitch rate. There was less correlation for line of sight and tracking error although the pilot model usually predicted the correct ranking of performance. Overall, the optimal pilot model was less successful in predicting short term tracking performance than it was in predicting long term performance.

UNCLASSIFIED

SECURITY CLASSIFICATION OF THIS PAGE(When Data Entered)